INSTITUTE OF PHYSICS PUBLISHING REPORTS ON PROGRESS IN PHYSICS

Rep. Prog. Phys. **66** (2003) 633–689 PII: S0034-4885(03)19196-8

Nuclear magnetic and quadrupole moments for nuclear structure research on exotic nuclei

Gerda Neyens

University of Leuven, Instituut voor Kern-en Stralingsfysica, Celestijnenlaan 200 D, B-3001 Leuven, Belgium

E-mail: gerda.neyens@fys.kuleuven.ac.be

Received 14 November 2002
Published 25 March 2003
Online at stacks.iop.org/RoPP/66/633

Abstract

One of the key issues in current nuclear physics research is to investigate the properties of so-called 'exotic nuclei' and of 'exotic nuclear structures'. Exotic nuclei are nuclei with a proton-to-neutron ratio that is very different from the proton-to-neutron ratio in stable nuclei (a technical term related to this ratio is the 'isospin'). We define exotic nuclear structures as excitation modes of nuclei that have a very different structure than the structure (or shape) of the nuclear ground state. By putting the nucleons in a nucleus to extreme conditions of isospin and excitation energy one can investigate details of one of the four basic forces in nature: the strong force which binds the nucleons together to form a bound nucleus. While the basic properties of the strong nucleon–nucleon interaction are known from investigating the properties of nuclei near the 'valley of stability', recent developments in the study of exotic nuclei have demonstrated that specific properties of the strong interaction, such as the influence of the spin-orbit term, are not yet understood. Because the nucleus forms a complex many-body system, it is impossible to describe it by *ab initio* calculations (except for a few very light nuclei, for which such calculations have become possible in the last few years) and therefore approximations need to be introduced. Several theoretical models have been developed in order to describe the properties of nuclei all over the nuclear chart. It is by measuring the basic nuclear properties such as masses, binding energies, lifetimes, excitation schemes, static and dynamic moments, and by comparing these properties to the predictions from the nuclear models, that these models can be tested and effective interactions can be improved. Furthermore, the measured nuclear properties can be a guide in understanding the changes, which the nuclear force undergoes in extreme conditions.

In this report, we focus on the electric and magnetic properties of a nuclear state, namely on what the static magnetic dipole and electric quadrupole moments can teach us about the nucleus as a system of independently moving particles in a central potential or as a system of collectively moving nucleons. We give an overview of some techniques to measure nuclear moments for a variety of nuclear states and we discuss how the recent developments in the production of exotic nuclei have influenced the development of new experimental tools for nuclear moment studies.

0034-4885/03/040633+57$90.00

Contents

1. Introduction

Nuclear moments have been studied since the very beginning of nuclear structure physics. The earliest measurements date back to the 1950s, when the nuclear magnetic moments of many stable nuclei were measured by the nuclear magnetic resonance (NMR) technique, a method that has evolved nowadays to a medical diagnostics tool known as magnetic resonance imaging (MRI). The measurement of nuclear quadrupole moments has always been—and still is—more difficult and challenging than magnetic moment measurements: the first quadrupole moments for stable nuclei have been reported since the 1960s. However, systematic studies on quadrupole moments of stable nuclei started only in the late 1970s, using mainly two techniques: the hyperfine structure of muonic x-rays or the atomic beam magnetic resonance method. In the same period, measurements on relatively long-lived radioactive nuclei started to appear as well. A complete 'table of nuclear moments', including all moments measured up to 1988, was prepared by Raghavan [1]. An update of this table, including moments measured up to 2001, is in preparation by Stone [2]. In both 'tables of nuclear moments' a list is given of all experimental techniques available to study moments of a wide variety of nuclear species: more than 40 different techniques have been exploited! Different properties of the nuclear structures of interest have advocated the development of all these methods: parameters such as the lifetime of the nuclear state (from picoseconds up to stable), the spin (from $\frac{1}{2}$ up to $30\hbar$ and more), its chemical properties, the way it was produced, its decay properties, all determined whether or not a particular method was suitable for the investigation of its nuclear moments.

It is not my aim to cover that history in this report. Instead I will concentrate on the developments that have been going on in this field during the past 15 years. Also nowadays, it is still necessary to develop new techniques—and to adapt existing methods—to the new production, selection and detection methods that have appeared in nuclear structure research the last two decades [3, 4]. With the appearance of the intermediate and high-energy projectile-fragmentation facilities combined with in-flight (IF) high-resolution mass spectrometers, a large variety of new nuclear species both on the proton and neutron-rich side of the nuclear chart became available for detailed spectroscopic investigations. Also the isotope separation on-line (ISOL)-based facilities have developed very rapidly in the last decade, following the pioneering work performed at Louvain-la-Neuve [5, 6]. Facilities like SPIRAL at GANIL, Caen, France [7], REX-ISOLDE at CERN, ISOLDE, Switzerland [8], HRIBF at ORNL, Tennessee, USA [9] and ISAC at Triumf, Canada [10] are nowadays providing pure high-quality radioactive beams which can be used not only for nuclear structure studies, but also will be very useful for other fields of fundamental research (fundamental interaction studies, nuclear astrophysics, nuclear solid state physics). At this very moment, projects worldwide are in preparation for building the next-generation radioactive beam facilities, both based on the IF as well as on the ISOL-based production schemes.

One of the reasons for these developments is the fact that most of our knowledge on the structure of atomic nuclei—containing more than 99.9% of the total mass of the universe—is based on the properties of nuclei close to the valley of stability. Only for about 500 nuclei have we measured most of their basic properties and can we explain them within a theoretical (but not universal) model. However, theoretical models predict that about 6000 types of nuclei might exist in our universe (being produced in the nuclear reactions and decay processes in stars) and the limits of existence are predicted very differently by various models. As soon as extremely exotic radioactive nuclei became available for experimentalists, new nuclear structure phenomena were discovered. The most striking example was certainly the discovery of the neutron halo structure in some very neutron-rich nuclei [11]. The foundations of the shell model were questioned as well, when it was found that good shell closures seemed to

disappear while new magic numbers seemed to appear instead [12–14] in nuclei far from stability. All these discoveries, of which the implications can be fully understood only by combining the results from many different types of experiments, have led to a variety of new theoretical developments [14–17]. In the last decade, theory and experiment have gone hand in hand in trying to understand the structure of the whole nuclear chart and in trying to come to a 'unified nuclear theory'. There is however still a very long way to go until that goal will be reached.

It is clear that to understand the nuclear structure, we need to measure as much as possible the properties of nuclei over a large range of isospin or make a detailed investigation of some specific 'key' nuclei. In this report, I will try to elucidate how the measurement of nuclear moments can help in understanding some aspects of nuclear structure. With just a few nuclei from one particular exotic isotope being experimentally available, it is of course not possible to measure nuclear moments. Therefore, nuclear moment measurements often come at the end, when other properties that require fewer nuclei, have been studied. However, even the nuclear moments can still reveal information that is not—or only indirectly—available from other properties. They allow confirmation of hypotheses which were based on indirect experimental evidence, or they can be a very valuable input in nuclear models for determination and testing of the model parameters.

The first thing to learn about an exotic nucleus is whether or not it is particle bound, in other words to determine the drip-lines of the nuclear chart. Only a few nuclei of an isotope are required to identify the new isotope as being particle stable, e.g. by using the energy-loss versus time-of-flight (TOF) techniques behind IF fragment separators [13]. The neutron drip-line has been fixed by now up to $Z = 9$ using this method [18]. Because the production of neutron-deficient nuclei is favoured in fusion–evaporation reactions, the proton drip-line has been reached much earlier. By using high-efficiency recoil mass separators and highly efficient γ arrays, the proton drip-line has been reached for several elements, including some heavy ones like $Z = 79$ [19]. If a few thousand isotopes are available for study, it is possible to determine the isotopic mass, its decay properties and its half-life. These properties are often first indications for possible changes in the nuclear structure (as compared to standard shell model predictions). Examples are the sudden changes in the two-neutron separation energies for neutron-rich nuclei around $N = 20$ and 28 [20, 21] suggesting the disappearance of these magic numbers respectively around $Z = 11$ and 16.

Once beams of exotic radioactive nuclei of about 10^3 s^{-1} can be produced (and purified), the way is open to study their nuclear spins and moments. These quantities provide us with very detailed information on the nuclear structure: while the magnetic moment is very sensitive to the single particle orbits occupied by the unpaired nucleons, the quadrupole moment is a unique tool to study the deformation and collective behaviour of nuclei both at low and high excitation energy. Both quantities can be directly compared with the predicted values in different nuclear models. They provide us with an excellent tool to test the validity of recently developed nuclear theories, and can help us to understand the basic ingredients needed to explain the changes in the nuclear shell structure.

This report will first demonstrate via some examples how the nuclear magnetic and quadrupole moment are sensitive to some features in the nuclear structure. The following three sections will be mainly technical, dealing with the production of the radioactive species of interest and the implication of that production mechanism to the kind of methods that can be applied for nuclear moment studies. An overview of available methods will be given with special attention to the recently developed methods, as well as to the complementarity of the techniques. As spin-orientation is a crucial issue in the study of nuclear moments, some techniques used for orienting the spins of radioactive nuclei will be discussed. In each of the

sections references to appropriate recent experimental results, coming out of the development of the last 10 years, will be given and a conclusion with a view on the future will be made.

2. Nuclear moments for probing changes in nuclear structure

A good introduction to the definitions and properties of nuclear moments is given in the book by Castel and Towner [22]. This book gives an introduction to nuclear moments and their connections to 'modern' nuclear theories. It discusses different aspects related to nuclear magnetic and quadrupole moments, such as single particle moments, core polarization effects, effective g factors and effective charges, etc. Here, I will concentrate on how one can deduce certain information out of nuclear moment measurements by illustrating this with a few examples.

A nucleus is a many-body system built out of nucleons (protons and neutrons). It is impossible to describe this quantum-mechanical few-body system with an exact wave function. Instead, each nucleon in the nucleus is considered as moving in an average potential created by all other nucleons. The eigenfunctions of the Schrödinger equation with this average potential are the so-called single particle orbits, characterized by the radial (n), the orbital (l) and the spin (j) angular momentum. A nucleus with Z protons and N neutrons will be constructed by filling these single particle orbits one by one for protons and neutrons separately, starting with the orbit having the lowest energy, and taking into account the Pauli exclusion principle. By adjusting the parameters of the average potential the ordering of the single particle orbits can be modified. As such it is possible to reproduce the well-known 'magic numbers' [23] as 'shell gaps' in the single particle level ordering, from which the name 'shell model' for this type of models arose. Nuclei with protons and/or neutrons equal to magic numbers exhibit special features. They have a reduced mass as compared to the liquid drop value and an increased energy of the first excited (often 2^+) state [24]. In the extreme single particle model, the properties of a nucleus with one proton (or neutron) outside a closed shell are determined fully by the properties of the orbit occupied by that odd proton (neutron). Thus, a detailed knowledge on the properties of nuclei with near-magic numbers are of crucial importance in the parametrization of the shell model interaction, especially their excitation energy scheme with spins and parities fixed for all levels.

The properties of a nucleus with several nucleons outside (or holes in) a closed shell will then be described in a first approximation by an inert core (e.g. a doubly magic nucleus) plus some nucleons which can move in a certain configuration space and which interact with the core and each other via a 'residual' interaction (particle–particle and particle–core interactions). Depending on the chosen model space and residual interactions, one can probe via comparison to several experimental parameters (excitation energy, spin/parity, magnetic and quadrupole moment) the validity of the model and parametrization of the residual interaction. The nuclear moments are often a good check if the parametrization and model space are appropriate. Deviations from the model predictions might indicate the presence of configuration mixing into other orbits (not taken into account in the chosen model space) or the need for other or better parameterized residual interactions. In the next paragraphs we will illustrate how, with nuclear magnetic and quadrupole moments, particular features of the nuclear structure can be directly probed and confirmed experimentally.

2.1. Nuclear magnetic moments

2.1.1. Definitions. The magnetic moment of a nuclear state with spin I is given by $\mu = gI\mu_N$, with g the nuclear gyromagnetic ratio. Experimental magnetic moments are always expressed

in units of the nuclear magneton μ_N (which may further be omitted). Note that some experimental methods measure the magnetic moment, while others measure the nuclear g factor. In both cases, it can be a way to deduce the unknown spin of an exotic nuclear state. This can be done by comparing the measured values to the values of similar states or by comparing the experimental magnetic moment (assuming a particular spin) to some model calculations. One has however to be very careful when doing this, as I will demonstrate later.

The magnetic operator $\bar{\mu}$ is a one-body operator and the magnetic dipole moment μ is the expectation value of $\bar{\mu}_z$. The M1 operator acting on a composed state $|\mathrm{Im}\rangle$ can then be written as the sum of single particle M1 operators $\bar{\mu}_z(j)$ acting each on an individual valence nucleon with total momentum j:

$$\mu(I) \equiv \left\langle I(j_1, j_2, \ldots, j_n), m = I \left| \sum_{i=1}^{n} \bar{\mu}_z(i) \right| I(j_1, j_2, \ldots, j_n), m = I \right\rangle \tag{2.1}$$

The single particle magnetic moment $\mu(j)$ for a valence nucleon around a doubly magic core is uniquely defined by the quantum numbers l and j of the occupied single particle orbit [22]:

$$\text{for an odd proton: } \begin{cases} \mu = j - \frac{1}{2} + \mu_p & \text{for } j = l + \frac{1}{2} \\ \mu = \dfrac{j}{j+1}\left(j + \dfrac{3}{2} - \mu_p\right) & \text{for } j = l - \frac{1}{2} \end{cases} \tag{2.2}$$

$$\text{for an odd neutron: } \begin{cases} \mu = \mu_n & \text{for } j = l + \frac{1}{2} \\ \mu = -\dfrac{j}{j+1}\mu_n & \text{for } j = l - \frac{1}{2} \end{cases} \tag{2.3}$$

These single particle moments calculated using the free proton and free neutron moments ($\mu_p = +2.793$, $\mu_n = -1.913$) are called the Schmidt moments. In a nucleus, the magnetic moments of the proton and neutron are obviously influenced by the medium (the presence of other nucleons), and therefore one will usually use 'effective' proton and neutron moments (g factors) to calculate the single particle moments. Corrections to the Schmidt moments include the influence of meson exchange currents (MEC) as well as first- and second-order core polarization effects [22] (some examples will be discussed later). All of these corrections can add up or cancel each other, depending on the case. In several mass regions, calculations have been performed to account for these types of deviations (e.g. in [25, 26] for orbits around the doubly magic ^{208}Pb). It is thus very important to measure the magnetic moments of states in [doubly magic +1] nuclei. Deviations of these values from the Schmidt values should arise totally from core polarization effects and MEC effects on the dipole moment operator, and not from configuration mixing effects.

Because the magnetic moment operator is a one-body operator, it allows us to deduce some general 'additivity' rules for the magnetic moment of a 'composed' nuclear state, provided that it can be described (in a simple model) with a few particles (and/or holes) around an inert core. The nuclear moments of an n-particle (m-hole) configuration are easily calculated from (2.1) by decoupling the wave function of a nuclear state with spin J into its single particle components (using Clebsch–Gordon coefficients [27] in the case of two particles and coefficients of fractional parentage for more particles [28]). For a nuclear state described by a weak coupling between protons and neutrons, the magnetic moment can be calculated as:

$$\mu(J) = \frac{J}{2}\left[\frac{\mu(J_\pi)}{J_\pi} + \frac{\mu(J_\nu)}{J_\nu} + \left(\frac{\mu(J_\pi)}{J_\pi} - \frac{\mu(J_\nu)}{J_\nu}\right)\frac{J_\pi(J_\pi+1) - J_\nu(J_\nu+1)}{J(J+1)}\right] \tag{2.4}$$

Examples of the additivity of nuclear magnetic moments are given in the book by Heyde [24]. Other such examples, as well as an example of the breakdown of the additivity rule, will be given in the next paragraphs.

Nuclear magnetic moments are very sensitive to which orbits are occupied by the valence particles (or holes). Magnetic moments thus provide a good test for the purity of a particular configuration. They are most sensitive to the orbits in which the unpaired particles are moving but very little sensitive to the number of paired particles or holes (as long as they are paired to zero spin). The influence of 2p–2h excitations on the magnetic moment is called second-order core polarization. As will be demonstrated with some examples, magnetic moments are not very sensitive to quadrupole particle–core coupling interactions (often inducing an increased deformation), in contrast to quadrupole moments which are extremely sensitive to this (see 2.2). Therefore, the magnetic moment is found to be constant in a chain of isotopes and for the same reason the magnetic moments are not very sensitive to whether an orbit is a 'normally' occupied orbit or whether it is an 'intruder' occupied orbit (which can be considered as a particle–hole excited state in a spherical shell model picture).

On the other hand, magnetic moments are very sensitive to mixing of spin-flip matrix elements into the wave function, e.g. configurations of the type $|\pi(l_{j-1/2}l^{-1}_{j+1/2}); 1^+\rangle$ (called first-order core polarization effects) will strongly influence the magnetic moment [25, 29]. Note that this type of configuration often involves a 1p–1h excitation across a magic shell gap (thus contributing very little to the wave function), but still they have a remarkable influence on the magnetic moment of these states. All these features of magnetic moments will be illustrated by a few examples.

2.1.2. Sensitivity to the valence particle configuration. The magnetic moment of an odd-mass nucleus can reflect the orbit occupied by the unpaired nucleon, provided that the nucleus can be described with a rather pure single particle wave function. In fact, it is the nuclear g factor that contains the orbit information, not the magnetic moment. This is illustrated in figures 1(*a*) and (*b*) where we compare the experimental magnetic moments and g factors of odd-mass ground states around the magic $Z = 82$ shell. Figure 1(*a*) shows the g factors for the ground states of the odd Au ($Z = 79$), Tl ($Z = 81$) and Bi ($Z = 83$) isotopes, as well as for some isomeric intruder $9/2^-$ states in the Tl isotopes. The Bi isotopes have one proton outside the closed $Z = 82$ shell. From the single particle levels in this mass region (figure 2) one can see that this proton will occupy the $\pi 1h_{9/2}$ orbit. Indeed, the spin and parity of the odd Bi ground states are $I^\pi = 9/2^+$ and the magnetic moments are in good agreement with a pure $\pi 1h_{9/2}$ configuration. The calculated single particle g factor, taking into account the first-order core polarization effects (due to 1p–1h spin-flip excitations) and the influence of MECs, gives $g_{\rm calc}(\pi 1h_{9/2}) = 0.91$, in good agreement with the experimental values [25] and much larger than the Schmidt value ($g_{\rm Schmidt} = 0.58$).

The g factor of the Tl ground states is very different because the wave function of these nuclei with one hole in the $Z = 82$ shell is dominated by a proton hole in the $\pi 3s_{1/2}$ orbit (thus having spin/parity $I^\pi = 1/2^+$). The calculated g factor $g_{\rm calc}(\pi 3s_{1/2}) = 3.08$ [25], taking into account only 1p–1h core polarization effects is in good agreement with most of the Tl g factors. Only for the $N = 126$ isotope a slight increase of the g factor towards the Schmidt value ($g_{\rm Schmidt} = 5.58$) is found, illustrating that in this nucleus with a closed neutron shell, the proton is less influenced by core polarization effects.

The g factors of the $9/2^-$ isomeric states in the neutron-deficient Tl isotopes are in a very good agreement with those of the $9/2^-$ states in the Bi isotopes. This is first of all a proof that these states have as a main configuration $|\pi h_{9/2}(2h)_0\rangle$, thus being a 1p–1h core-excited state (also called 'intruder' state because as a function of deformation, the $\frac{9}{2}$ orbit has a steep down

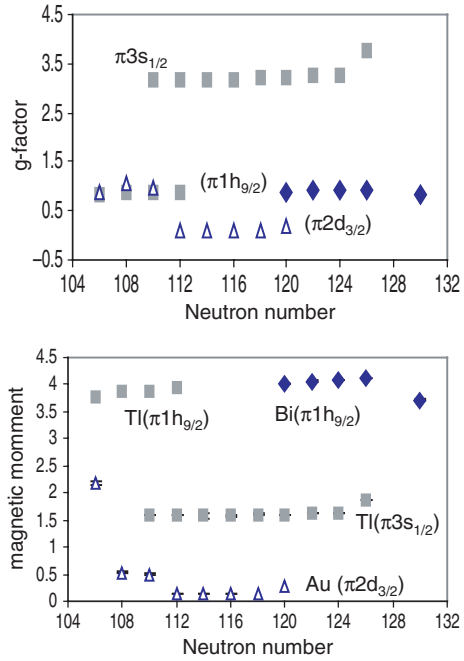

Figure 1. Experimental g factors and magnetic moments of odd-mass $Z = 79$ (Au), 81 (Tl), 83 (Bi) ground states (from [1, 2, 33]) and isomeric intruder states in Tl, illustrating the sensitivity of g factors to the orbit occupied by the valence proton and of the magnetic moments to changes in the structure. The magnetic moment is almost completely insensitive to nuclear deformation and to second-order core polarization (particle–core coupling and mixing with 2p–2h excitations), by which the g factors are very constant over a wide isotopic chain. The magnetic moment is very sensitive to first-order (1p–1h) core polarization effects and MECs, being the main explanation for the deviation from the Schmidt values. If error bars are missing, they are smaller than the dot.

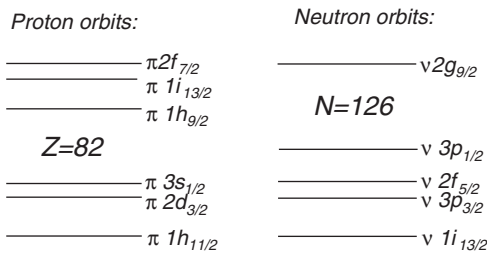

Figure 2. Proton and neutron single particle orbits around the doubly magic nucleus ^{208}Pb.

going slope (intrudes) into the positive parity orbits below $Z = 82$). It also illustrates that, as explained before, the g factor is not strongly sensitive to the deformation. Also the fact that the proton g factors are very constant over a wide range of isotopes for both elements, illustrates the small sensitivity to second-order core polarization effects (mixing with particle–core coupled configurations in which a valence nucleon couples to a low-lying collective excited state of the core).

On the other hand, the g factors of the Au ground states are changing quite drastically with neutron number: at $N = 110$ a huge change of the g factor reflects a clear change in their ground state structure. Above $N = 110$ the g factor is close to the Schmidt value for

a $\pi 2d_{3/2}$ orbit ($g_{\text{Schmidt}} = 0.2883$) in agreement with the fact that the ground state spins are indeed $I = \frac{3}{2}$ and mainly dominated by a hole in the $\pi 2d_{3/2}$ orbit. As the g factors of the $N \leqslant 110$ Au isotopes agree very well with the g factors for the Bi isotopes, this suggests that, when approaching neutron mid-shell, the ground state of the Au-isotopes is dominated by the intruder proton $\pi 1h_{9/2}$ orbit [30]. Concluding from this that the ground state spin thus changes from $I = \frac{3}{2}$ to $I = \frac{9}{2}$ at $N = 110$ is however a too fast conclusion!

In figure 1(*b*), we compare the magnetic moments of these states. The magnetic moment depends both on the spin and the g factor. As long as both the spin and the g factor remain constant, the valence proton configuration does not change drastically. A sudden jump in μ is an indication for a structure change. Between $N = 106$ and 108 it is due to a change in spin (being $I = \frac{5}{2}$ for $^{185}Au_{106}$ and $I = \frac{1}{2}$ for $^{187}Au_{108}$ and $^{189}Au_{110}$ [31]), although the g factors show that the same orbit remains occupied. So, attributing a spin based on a g factor measurement is only possible if the nuclear state is not too much deformed and if it can be described in a spherical shell model: only then the spin of the odd proton is defined by the j-quantum of the valence orbit. The drastic shape changes in the Au nuclei have been confirmed by measurements of the mean square charge radii, from which a sudden increase of the deformation from 0.15 to 0.25 is found at $N = 107$ [32] (and no change at $N = 110$ as might be wrongly deduced from the g factor).

2.1.3. Sensitivity to second-order core polarization. In figure 3, we compare the magnetic moments of odd-neutron states with spin/parity $I^{\pi} = 13/2^{+}$ (mainly dominated by the $\nu 1i_{13/2}$ orbit) in the odd isotopes of Hg ($Z = 80$), Pb ($Z = 82$) and Po ($Z = 84$). Again a very similar value is found for each of these g factors, changing not more than 10% around an average value. The systematic decrease as a function of N, which is visible in the Pb-chain, has been attributed to an increasing first-order core polarization [29]. The more neutrons occupy the $\nu 1i_{13/2}$ orbit, the higher the core polarization correction (which in this case gives a higher deviation from $g_{\text{Schmidt}} = -1.913$).

For the lighter Hg-isotopes a deviation towards lower neutron numbers appears as well, which might indicate that the correction is rather related to the maximum of particles or holes, which is minimal when half the orbit is filled. That seems to occur at different neutron numbers for Pb and Hg-isotopes. Notice that the magnetic moment of the Pb-isotopes is closer to the Schmidt value ($g_{\text{Schmidt}} = -1.913$) than in the Po and Hg-isotopes having, respectively, 2 holes inside and 2 particles outside the closed $Z = 82$ shell. This has been explained by an increase of second-order core polarization in the non-magic nuclei.

The trend of g factors of proton configurations as a function of neutron number reveals very little sensitivity to the second-order core polarization. In particular, the sensitivity to the

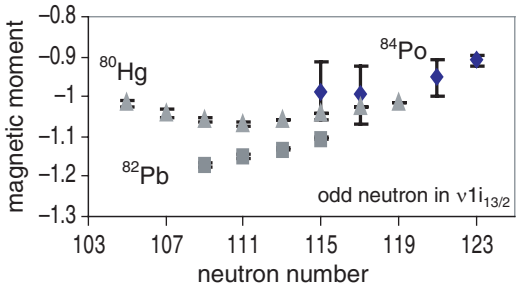

Figure 3. Magnetic moments of the $I = \frac{13}{2}$ neutron states in odd Hg, Pb and Po isotopes.

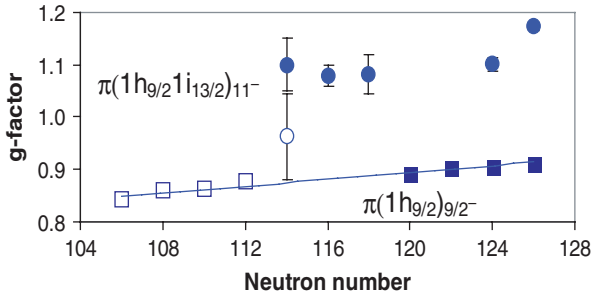

Figure 4. Experimental g factors of normal (dark) and intruder (light) proton-states in Bi and Tl, and in Po and Pb. Data are taken from [1, 2].

'normal' or 'intruder' character of a nuclear state is very low, as illustrated in figure 4 where the g factors of $I = 9/2^-$ ground states in odd Bi isotopes (filled squares) are compared to the g factors of intruder $I = 9/2^-$ states in the odd Tl isotopes (open squares). A similar comparison is made for the 'normal' 11^- isomeric states in the even Po isotopes (filled circles) and the 'intruder' 11^- state in ^{196}Pb (open circle). Because the measurements on the $9/2^-$ states have been performed with a high accuracy [33], we can draw following conclusions:

- the $\pi h_{9/2}$ g factors are decreasing with decreasing neutron number. As explained in section 2.1.2 the single particle g factor for a $\pi h_{9/2}$is well reproduced near $N = 126$, taking into account the first-order core polarization in the dipole operator ($g_{\rm calc} = 0.91$). The fact that the g factors approach more closely the Schmidt value ($g_{\rm Schmidt} = 0.58$) when going away from the closed shell, can be attributed to a negative contribution of the second-order core polarization effects, which become more important with increasing number of holes in the $Z = 126$ shell.
- A trend line is drawn through the Bi g factors. The Tl g factors follow exactly this trend line, which allows to conclude that breaking the $Z = 82$ closed shell does not induce a significant change of the g factor. Although the deformation of the Bi and Tl isomers is significantly different (as can be concluded from their quadrupole moments, section 2.2), the g factor is very similar. The g factor is thus not very sensitive to core polarization effects related to the breaking of the proton core.

The g factor of the 11^- intruder isomer in ^{196}Pb seems smaller than in its isotone ^{198}Po. However, the error bar on both values is rather large, and a more accurate measurement is needed in order to draw a conclusion on the sensitivity of the 11^- g factors to the nature (deformation) of these isomeric states. If we consider a similar behaviour for the 11^- as for the $9/2^-$ states, the g factor of the ^{196}Pb isotone would be around $g(11^-) = 1.09(2)$. Notice that in a recent measurement of the quadrupole moment of these 11^- intruder states [34], a g factor of 0.96(8) was assumed to deduce the quadrupole moment from the measured Q/μ ratio. Thus, a larger magnetic moment of this intruder isomer would lead to a larger quadrupole moment as well.

A re-measurement of this intruder state g factor is thus of importance!

2.1.4. Additivity of the M1-operator and first-order core polarization. An illustration of the additivity of the magnetic moment operator (or rather the breakdown of it) can be demonstrated via the g factors of isomeric states in the closed $N = 126$ isotones of Bi, Po, At, Rn, Fr and Ra. According to the additivity rule, the g factors of these isomeric states with a rather pure

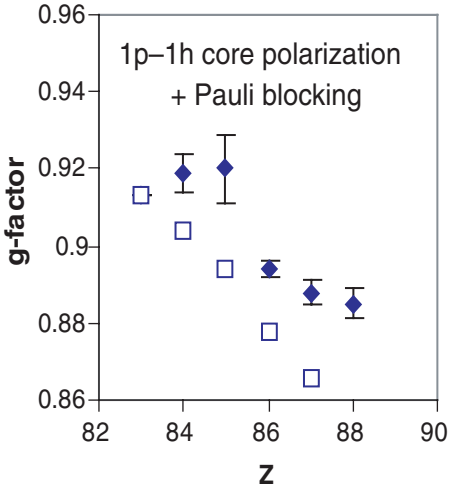

Figure 5. Experimental g factors of 8^+, $9/2^-$ and $21/2^-$ isomers in $N = 126$ isotones above Pb. As the main configuration of these high-spin isomers is expected to be $\pi(1h_{9/2})^n$, the g factor of these isomers should be the same for all of them (additivity theorem). The deviation from this additivity can be explained by a subtle interplay between first-order core polarization blocking (which is overestimated as shown by the □) and configuration mixing, including particle–core coupling to octupole vibrations of the Pb-core. A detailed discussion can be found in [36].

$\pi(1h_{9/2})^n$ configuration (coupling to spins $J = 8$ and $J = \frac{21}{2}$) should all be the same [28]. Figure 5 shows that the experimental moments are not in agreement with this additivity rule, but decrease towards the Schmidt moment with increasing Z. It is known that the configurations of these isomers are getting more mixed with increasing Z, in particular mixing with the $|\pi[1h_{9/2}^{n-1}2f_{7/2}]J^\pi\rangle$ configuration (figure 2). However, this mixing alone is not able to explain the breakdown of additivity. Other types of configuration mixing and/or core polarization effects are needed to account for the deviation from additivity. Many theoretical studies have been performed over the last 30 years, trying to account in a consistent manner for this breakdown of additivity. Arima and Hyuga [26] showed in 1979 that the influence of meson exchange effects and the influence of higher order core polarization effects cancel each other. This means that basically only first-order corrections (spin-flip configurations coupled to valence particles such as $|\pi[(1h_{9/2}^n)_{J^\pi} \otimes (1h_{9/2}^1 h_{11/2}^{-1})_{1^+}]J^\pi\rangle$) remain to explain the variation of the g factor with increasing number of protons. Because of the increasing occupation of the $h_{9/2}$ with increasing Z, fewer excitations from $h_{11/2}$ into that orbit are possible (by Pauli principle), thus reducing this core polarization contribution such that the g factor tends towards the Schmidt value at higher Z. However, this Pauli-blocking of the core polarization, calculated by Towner *et al* [35] is too strong (the experimental g factors drop much slower as demonstrated in figure 5). Stuchbery *et al* [36] show that not only 1^+ particle–core coupling configurations are contributing to first-order corrections in the M1 operator. In these nuclei, due to the mixing between $|(h_{9/2})^n; J\rangle$ and $|(h_{9/2})^{n-1}f_{7/2}; J\rangle$ in the isomeric wave functions, also configurations in which the valence particles couple to octupole-vibrations of the underlying core (configurations of the type $|[(h_{9/2})^{n-1}i_{13/2}]_{11^-} \otimes 3^-]; 8^+\rangle$) need to be taken into account in the wave functions. As the configuration mixing is increasing with increasing number of protons, the octupole mixing mechanism predicts g factors that increase with Z. This trend is the opposite of that predicted by core polarization blocking. Combining multiparticle–octupole coupling and first-order core polarization blocking therefore significantly reduces the discrepancy between the experimental and theoretical g factors of these states. The main effect

of the octupole mixing into the wave function is that fewer protons are occupying the $h_{9/2}$ orbit, resulting in a reduced Pauli blocking and thus better agreement with the experimental data. This demonstrates how subtle effects of core polarization and configuration mixing can have opposite effects on the nuclear g factor.

2.1.5. Conclusions. To conclude this section, let me summarize a few properties of nuclear dipole moments and g factors:

(a) the M1 operator is a one-body operator, leading to the 'addivity-rule' of g factors. This allows a particular configuration to be attributed to a particular nuclear state, provided that the nuclear state can be described by a rather pure (single- or multi-particle/hole) configuration. That is most often the case for high-spin excited states in nuclei close to magic numbers, having a high-spin due to alignment of the single particle spins.
(b) The magnetic moment in heavy nuclei is not very sensitive to second-order core polarization effects. That means that it is not sensitive to coupling of valence particles to quadrupole vibrations (E2) of the core or to 2p–2h excitations in the core. That is illustrated by a constant g factor over a long chain of isotopes in the Pb-region, as well as a similar g factor for 'normal' and 'intruder' states.
(c) The g factor in intermediate and heavy nuclei is very sensitive to M1 particle–core coupling, mainly to coupling of valence particles to spin-flip matrix elements (1p–1h excitations between spin-orbit partners across a major shell). This 'first-order core polarization' effect is a major cause for deviation of the single particle g factors from the Schmidt moments (free g factors) in heavy nuclei.
(d) First-order core polarization can be blocked in some isotopes, e.g. due to the Pauli principle. This can give rise to 'core polarization Pauli-blocking' causing a breakdown of the 'additivity rule' for g factors, resulting in a changing g factor as a function of Z or N.
(e) Single particle g factors deviate from the free-nucleon g factors also because of the presence of MECs between the nucleons in a core. As a consequence, the magnetic dipole operator has to be modified into an 'effective' M1 operator which takes into account this meson currents. An extended discussion on MECs can be found in [22] and references therein.

2.2. Nuclear quadrupole moments

2.2.1. Definitions. The spectroscopic quadrupole moment Q_s of a nuclear state with spin I is a measure of the deviation of the nuclear charge distribution from sphericity. The electric quadrupole moment operator $\bar{Q}$ is defined as

$$\bar{Q} = e \sum_{k=1}^{A} (3z_k^2 - r_k^2)$$

with e the electric charge and (z_k, r_k) the position coordinates of the kth nucleon [22]. The spectroscopic quadrupole moment is the expectation value of $\bar{Q}_z$ defined as:

$$Q_s(I) \equiv \langle I, m = I | \bar{Q}_z | I, m = I \rangle \equiv \sqrt{\frac{I(2I-1)}{(2I+1)(2I+3)(I+1)}} \langle I \| \bar{Q}_z \| I \rangle \tag{2.5}$$

It can be expressed as a function of the reduced matrix element using the Wigner–Eckart theorem [28], which immediately visualizes that for $I = \frac{1}{2}$ nuclear states the spectroscopic quadrupole moment is zero (although its intrinsic moment is non-zero). In a shell model picture, the wave function $|\mathrm{Im}\rangle$ of a nuclear state is determined by the configuration of the

valence particles. Therefore, the sum of all A nucleons in (2.5) is reduced to the sum over the valence nucleons only. Due to this, the free-nucleon charges ($e_\pi = 1$ and $e_\nu = 0$) need to be modified into effective charges $e^\pi_{\rm eff}$ and $e^\nu_{\rm eff}$, to account for the influence of particle–core and particle–particle residual interactions and particular configuration mixings that have not been taken into account into the wave function.

The E2-operator is often expressed as a function of the spherical tensor components $Y^0_2(\theta_k\varphi_k)$:

$$\bar{Q} = \sum_{i=1}^{n} \bar{Q}_z(i) = \sqrt{\frac{16\pi}{5}} \sum_{i=1}^{n} e^i_{\rm eff} r_i^2 Y^0_2(\theta_i, \varphi_i) \tag{2.6}$$

with n the number of valence nucleons. As the quadrupole operator is a one-body operator, the quadrupole moment of a multi-valence particle state can be expressed in terms of the single particle moments, by applying angular momentum decoupling rules [24]. The single particle quadrupole moment $Q_{\rm s.p.}(j)$ of a nucleon in an orbit with spin j depends on the radial and angular properties of the orbit:

$$Q_{\rm s.p.} = -e_j \frac{2j-1}{2j+2} \langle r_j^2 \rangle \tag{2.7}$$

with $\langle r_j^2 \rangle$ the mean square radius for a particle in the orbit (n, l, j). A particle moving outside a closed shell thus has a negative quadrupole moment and can be interpreted as polarizing a spherical core towards an oblate deformation. If a hole is considered in an orbit, the quadrupole moment changes sign (e_j(hole) $= -e_j$(particle)). Examples of calculated single particle quadrupole moments in the Pb-region are given by Sagawa and Arima [37] for states with one particle/hole around the doubly magic ^{208}Pb. They calculated the effective charges taking into account particular particle–core coupling interactions in the framework of a microscopic theory. A good agreement with the experimental quadrupole moments of closed-shell $+1(-1)$ nuclear states is found, as illustrated in table 1 and figure 6(a). In figure 6(b), the effective single particle quadrupole moments are calculated using a universal effective charge for protons $e^{\rm eff}_\pi = 1.5e$ and for neutrons $e^{\rm eff}_\nu = 0.95e$. These effective moments are in good agreement with all experimental values, illustrating that a universal effective charge for protons and neutrons can be used in this mass region. However, a more accurate measurement of the $\pi\,1i_{13/2}$ quadrupole moment, as well as an experimental value of the $\pi\,2f_{7/2}$ quadrupole moment are highly desirable in order to unambiguously exclude an orbital dependence of the proton effective charge.

The quadrupole moment is an excellent tool to study the deformation of nuclei. For well-deformed axially symmetric nuclei, the measured (= spectroscopic) quadrupole moment $Q_{\rm s}$ can be related to the intrinsic quadrupole moment Q_0 through the relation:

$$Q_{\rm s} = \frac{3K^2 - I(I+1)}{(I+1)(2I+3)} Q_0 \tag{2.8}$$

This is valid in the strong coupling limit, with K the projection of the total spin I onto the symmetry-axis of the deformed nucleus. In the hydrodynamical model of the nucleus (where the nucleus is considered to be a liquid drop), the intrinsic quadruple moment is related to the nuclear deformation parameter β_2 as follows [37]:

$$Q_0 = \frac{3}{\sqrt{5\pi}} eZR^2\beta_2 \left\{ 1 + \pi^2 \left(\frac{a}{R}\right)^2 + \frac{2}{7}\sqrt{\frac{5}{\pi}}\beta_2 \right\} \tag{2.9}$$

This expression takes into account a correction due to the surface thickness ($a = 0.54$ for the Pb region) and the nuclear radius is taken as $R = 1.2A^{1/3}$ fm. The surface correction term is often not taken into account because it is very small, in particular for heavy nuclei. In this report, we will therefore neglect this correction. A review of the different definitions of deformation parameters can be found in [40].

Table 1. Core polarization charges $e_{\rm eff}$(calc) for single particle orbits around doubly magic ^{208}Pb calculated by Sagawa and Arima [37]. The mean square charge radii are calculated with the Hartree–Fock radial wave functions. Using expression (2.7) and the calculated effective charges and radial wave functions, the theoretical single particle quadrupole moments are obtained. A universal effective proton charge $e_\pi^{\rm eff} = 1.5e$ and neutron charge $e_\nu^{\rm eff} = 0.95e$ is used to calculate $Q_{\rm eff}$-values which are in a good agreement with the experimental quadrupole moments (see also figure 6(*b*)). The experimental values are deduced from isomeric state quadrupole moments around ^{208}Pb.

Single particle orbit		$\langle r^2\rangle$	$e_{\rm eff}$(calc)	$Q_{\rm theo}$ (efm^2)	$Q_{\rm eff}$ (efm^2)	$Q_{\rm exp}$ (efm^2)	Reference
					$e_\pi^{\rm eff} = 1.5e$		
Protons	$1i_{13/2}$	42.2	1.68	−56.8	−50.6	−45(11)	[38]
	$2f_{7/2}$	35.55	1.66	−39.3	−35.6		
	$1h_{9/2}$	36.36	1.52	−40.1	−39.7	−37.0(2.6)	[1]
						−41.5(1.5)	[38]
					$e_\nu^{\rm eff} = 0.95e$		
Neutrons	$2g_{9/2}$	41.75	0.835	−25.4	−28.7	−29.3(1.6)	[39]
	$(2f_{5/2})^{-1}$	35.98	−0.945	19.4	19.4	22.6(3.7)	[1]
	$(1i_{13/2})^{-1}$	40.25	−0.946	30.5	30.4	30(5)	[1]

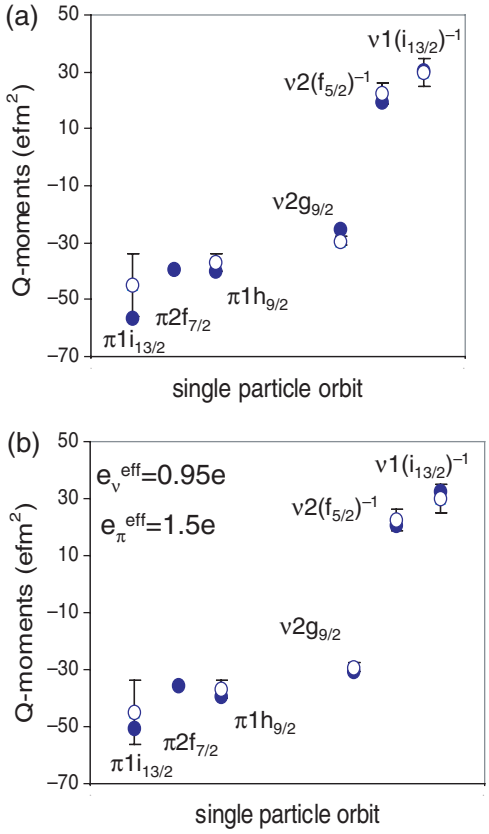

Figure 6. Experimental quadrupole moments of isomeric single particle states around ^{208}Pb compared to calculated single particle moments (see table 1 and text for explanation): (*a*) effective charges for individual orbits calculated by Sagawa and Arima [37] (*b*) using a universal proton and neutron effective charge, respectively, $e_{\rm p} = 1.5e$ and $e_{\rm n} = 0.95e$.

2.2.2. Sensitivity to the core softness and shape coexistence in near-spherical nuclei. The effective charges calculated in [37] are for valence particles in [doubly magic ± 1] nuclei. Measurements of quadrupole moments of isomeric and ground states in the more neutron-deficient isotopes in this mass region have revealed a systematic increase of the quadrupole moments with decreasing neutron number [41–46]. This increase is a signature for the increase of the nuclear deformation, attributed to an increasing quadrupole collectivity induced by interactions between the proton particles and holes in the neutron shell. In figure 7, the experimental quadrupole moments of several isomeric states in the neutron-deficient trans-lead region are presented, normalized to the value of their $N = 126$ isotone. A similar trend is seen for all isomers, independent of the proton configuration. It means that the core polarization is similar for all proton orbits around $Z = 82$. For very neutron-deficient nuclei, the core polarization correction becomes even larger than the quadrupole moment of the valence particles. A saturation seems to occur around $N = 114$, where a constant relative effective charge $e_\pi^{\rm eff}(N)/e_\pi^{\rm eff}(N = 126) \sim 2.4$ appears (as deduced from the relative quadrupole moments in figure 7). It has been shown in [47] that this increase of the quadrupole moments can be well described by taking into account the coupling of the valence protons to quadrupole vibrations of the underlying Pb core, in a similar way to that described in [24]. The residual interaction that gives rise to a neutron dependent quadrupole core polarization can be estimated from the 2^+ excitation energy and B(E2, $0^+ \rightarrow 2^+$) transition probabilities in the respective Pb isotones. Because not enough experimental B(E2) values are available to calculate the neutron-dependent proton effective charge down to $N = 116$ [47], further calculations in this report will be done using an empirical proton effective charge $e_\pi^{\rm emp}(N)$, obtained from fitting the data points in figure 7. The deduced values are presented in table 2.

Note that for the most neutron-deficient isomers in figure 7, the configurations only involve $\pi h_{9/2}$ protons. For isomers in which the protons occupy also the $\pi 1i_{13/2}$ orbit, no static quadrupole moments could be derived so far. Transitional moments have been derived for some $\pi(1h_{9/2}\ 1i_{13/2})11^-$ isomers in Po, around neutron number $N = 114$. An enhanced E3-transition probability has been observed between the 11^- and $\pi(1h_{9/2}^2)8^+$ isomers, both in the Po [48] as well as in the Pb isotopes [49]. In the Pb nuclei, this isomer has an 'intruder' 2p–2h character $\pi(3s_{1/2}^{-2}\ 1h_{9/2}\ 1i_{13/2})$. It was suggested that an additional coupling to octupole vibrations needs to be taken into account [49] for these configurations, in order to explain this enhanced transition probabilities. This seems to be confirmed by a recent measurement of the static quadrupole moment of the intruder 11^- isomers in ^{194,197}Pb and calculations within the particle–core coupling model [50]. In a simple two-level mixing model including only

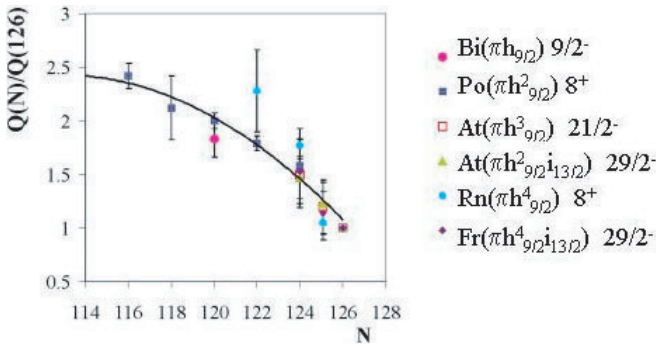

Figure 7. Quadrupole moments of isomeric states with different proton configurations, relative to the experimental value at $N = 126$. The data are taken from [1, 33, 42–45, 47].

Table 2. Empirically deduced proton effective charge as a function of neutron number (from the fit to data in figure 7). The effective charge increases with the number of holes in the $N = 126$ shell, reaching saturation around $N = 114$ where the proton effective charge is about 2.4 times larger than at $N = 126$. The effective charge at the closed neutron shell is chosen as $e_\pi^{\rm eff}(N = 126) = 1.5$ (from table 1).

N	$e_\pi^{\rm emp}(N)/e_\pi^{\rm emp}(126)$	$e_\pi^{\rm emp}(N)$ (e)
126	1.10	1.64
125	1.30	1.94
124	1.48	2.22
123	1.65	2.47
121	1.80	2.70
120	1.94	2.90
119	2.06	3.09
118	2.16	3.24
117	2.25	3.38
116	2.32	3.48
115	2.38	3.57
114	2.42	3.63

quadrupole vibrations, the theoretical moments are smaller and in less good agreement with the data than the calculations including a more extended configuration space. Measuring the quadrupole moments of the 'normal' Po 11^- isomers, which have a regular character, should reveal more directly the possible influence of octupole vibrations on the nuclear deformation. Note that the particle–octupole coupling starts to play a significant role in nuclei where the enhanced E3-transition probability is seen, this is at $N = 114$ [49]. This is also the region where the deformation of the core is getting stabilized according to figure 7 (and a similar effect can be deduced from figure 8 for neutron states, next paragraph).

To make the link between the static spectroscopic quadrupole moment and the nuclear charge deformation, we need to make some assumptions, which are validated by experimental evidence. For nearly-spherical nuclei, the quadrupole moment is mainly determined by the odd valence particles, giving rise to a small oblate core polarization. This turns into a small static core deformation when sufficient neutrons are taken out of the $N = 126$ shell, as demonstrated in figure 7 for proton configurations and in figure 8 for neutron configurations. We can deduce this deformation from the measured quadrupole moments, assuming strong coupling with $K = I$ (that means the nuclear spin along the oblate symmetry-axis). Following [37, 43] we have calculated the core deformation $\beta_2^{\rm core}$ using expression (2.9). The intrinsic quadrupole moment of the core is obtained from the spectroscopic core quadrupole moment $Q_{\rm s}^{\rm core} = Q_{\rm exp} - Q_{\rm s.p.}(j, N = 126)$ using relation (2.7). The single particle quadrupole moments are calculated from expression (2.7) and are given in table 1 for the relevant orbits. Typical values for the core deformations vary between $|\beta_2^{\rm core}| = 0.01$ up to $|\beta_2^{\rm core}| = 0.05$ for all high-spin isomers in the $Z = 82$–88 nuclei down to $N = 116$. Also for neutron core-excited isomeric states in At [43] and Fr [44], the core deformation is not larger than $\beta_2^{\rm core} = -0.055$, suggesting that neutron excitations across the $N = 126$ shell gap do not induce an extra deformation.

If the deformation of the isomeric state is directly deduced from the experimental quadrupole moments, values up to $\beta_2 = -0.065$ are found for the $N = 116$ Po isomers, while for the neutron core-excited isomeric states, the deformation goes up to $\beta_2 = -0.075$. Only a slight increase as compared to the core deformation is found, which confirms the fact that the deformation of the isomeric states with holes in the $N = 126$ shell is mainly determined by the core part, and very little by the valence particles. Configurations including core-excitations

across the $N = 126$ shell gap into the $\nu 1i_{11/2}$ and $\nu 2g_{9/2}$ orbits are slightly more deformed, but cannot yet be considered as well-deformed nuclei (having typically $|\beta_2| > 0.15$).

In the very neutron-deficient Pb-isotopes (below $N = 118$), core-excited isomeric states occur as well. In these magic $Z = 82$ nuclei with several holes in the $N = 126$ shell, protons are excited across the $Z = 82$ shell gap into the $\pi 1h_{9/2}$ and $\pi 1i_{13/2}$orbits, coupling to 11^- 'intruder' isomeric states. These high-spin proton core-excited isomeric states have a similar 2p–2h configuration as the 'intruder' 0^+ states that appear in these nuclei [51, 52] and which were predicted to be significantly deformed around $\beta_2 \sim -0.17$ [53]. The large deformation of these nuclear states suggests that they belong to a different potential well than the 'normal' nearly-spherical states in these nuclei. Such a phenomenon of different nuclear shapes appearing in the same nucleus is called 'shape coexistence' [53, 54]. The strong oblate deformation is induced by the strong 'intrusion' of the $\pi 1h_{9/2}$ and $\pi 1i_{13/2}$ orbits into the levels below $Z = 82$. A direct measurement of the deformation of these intruder states has been performed only recently via the determination of the isomeric quadrupole moments of 11^- intruder isomers in ^{194,196}Pb [34, 55]. Deformations of the order of $\beta_2 = -0.16(3)$ have been deduced, in very good agreement with the theoretical predictions and confirming the shape coexistence in semi-magic quasi-spherical nuclei.

So, while the neutron excitations across the $N = 126$ gap seem not to give rise to shape coexistence, proton excitations across the $Z = 82$ gap have been proven to induce a moderate oblate deformation of these states, which coexist with nearly-spherical states.

2.2.3. The quadrupole moment for n particles in an orbit. When n valence particles (holes) in an orbit j are coupling to a total spin J, the quadrupole moment of such a pure configuration $|j^n; J\rangle$ can be calculated in a seniority model [28] using properties of tensor algebra and angular momentum coupling rules. As an example, we consider the quadrupole moment of a n-particle, seniority $\nu = 2$ configuration (so two of the valence nucleons are unpaired), which can be expressed as a function of the quadrupole moment of the two-particle configuration $Q(|j^2; J\rangle)$, using the following relation between reduced E2-matrix elements:

$$\left\langle j^n; \nu J \left\| \sum_{i=1}^{n} Q_z(i) \right\| j^n; \nu J \right\rangle = \frac{2j+1-2n}{2j+1-2v} \left\langle j^2; \nu J \left\| \sum_{i=1}^{2} Q_z(i) \right\| j^2; \nu J \right\rangle \tag{2.10}$$

This relation illustrates that the quadrupole moments of nuclear states described by a pure $|j^n; \nu J\rangle$ configuration should follow a simple linear relation. Furthermore, it is possible to express the two-particle quadrupole moment as a function of the single particle quadrupole moment using reduction rules for tensor operators [24]:

$$\left\langle j^2; J \left\| \sum_{i=1}^{2} Q_z(i) \right\| j^2; J \right\rangle = (2J+1)(-1)^{2j+J} \begin{Bmatrix} j & J & j \\ J & j & 2 \end{Bmatrix} \langle j \| Q_z(i) \| j \rangle \tag{2.11}$$

We can verify this additivity rules, e.g. for the 12^+ and $13/2^+$ isomers in the $Z = 82$ (Pb) and the $Z = 80$ (Hg)-isotopes. For isotones between $N = 118$ and 108, we expect in a spherical shell model picture, that nuclear states with neutron holes in the $\nu 1i_{13/2}$ orbit (figure 2) appear at rather low excitation energy. In the even isotopes their main configuration is expected to be $|\nu(1i_{13/2})^n; \nu = 2, 12^+\rangle$, and in the odd isotopes it is $|\nu(1i_{13/2})^{n-1}; 13/2^+\rangle$. The 12^+ isomers are found to be short-lived (typically ~100 ns) and occur at about 2 MeV excitation energy (energy needed to break up the neutron pair), while the unpaired $\nu 1i_{13/2}^{-1}$ hole gives rise to a very long-lived isomeric state ($T_{1/2} \sim$ min) occurring only 100 keV above the low-spin ground state [1]. Using the reduction rule (2.11) we can deduce from the 12^+ quadrupole moments the quadrupole moment of the odd $\nu 1i_{13/2}$ neutron: $Q(12^+) = 1.54\,Q(\nu 1i_{13/2})$.

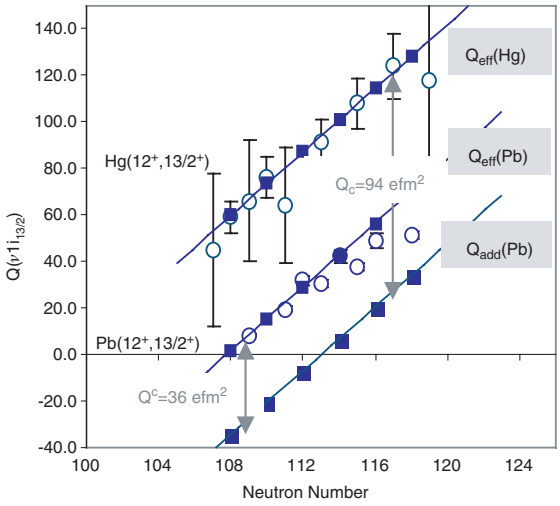

Figure 8. Experimental quadrupole moments (○) of the 12^+ and $13/2^+$ isomeric states in Pb and Hg (from [1, 2]) compared to the additivity rule (■). The $Q(12^+)$ have been reduced to $Q(13/2^+)$ using relation (2.11) (see text for more details).

In figure 8, we plot the experimental quadrupole moments $Q(\nu 1i_{13/2})$ as a function of neutron number. The values are the measured $Q(13/2^+, N \text{ odd})$, while in the even isotopes the $Q(i_{13/2}, N \text{ even})$ is deduced from the experimental $Q(12^+)$. The values are compared to the additivity rule (2.10), rescaled to the single particle quadrupole moment using (2.11). According to the spherical shell model, the number of particles in the $\nu 1i_{13/2}$ orbit is $n = 12$ at $N = 118$ down to $n = 2$ in $N = 108$ (figure 2). For the single particle quadrupole moment in expression (2.11) we used the pure single particle value from (2.7) assuming $e = 1$ and calculated with the radial wave functions from table 1, $Q_{\text{s.p.}}(\nu 1i_{13/2}) = -33.2\,\text{efm}^2$. The additivity quadrupole moments Q_{add} obtained in this way are represented as large full squares in figure 8. The trend line agrees very well with the experimentally observed one. However, while theoretically the quadrupole moment should be zero at mid-shell, this is not observed experimentally. In fact, the experimental values are very well reproduced by adding a constant quadrupole moment $Q_c(\text{Pb}) = 36(1)\,\text{efm}^2$ and $Q_c(\text{Hg}) = 94(2)\,\text{efm}^2$, leading to the effective quadrupole moments $Q_{\text{eff}} = Q_{\text{add}} + Q_c$ in figure 8. This constant additional deformation can be interpreted as a constant core deformation, which is found to be small for these two-neutron states: $\beta_2^{\text{core}}(\text{Pb}) = +0.016(1)$ and $\beta_2^{\text{core}}(\text{Hg}) = +0.047(1)$. From this result, we can conclude that:

(a) the isomeric states based on the $1i_{13/2}$ orbit in neutron-deficient Hg and Pb isotopes have a small prolate deformation, respectively, $\beta_2 \sim 0.09$ and $\beta_2 \sim 0.03$, due to core polarization by the neutron holes in the $N = 126$ shell. The isomers in the Hg isotopes exhibit a much stronger core polarization because they have 2 holes in the $Z = 82$ shell. However, their deformation is not yet as large as for a real 'deformed' state.

(b) The trend of the isomeric quadrupole moments in both isotopes is well reproduced assuming the additivity rule for n particles filling an orbit. Adding a constant core polarization allows to obtain a perfect quantitative agreement as well, at least for the Hg isotopes. This suggests a slightly prolate deformed core for these neutron states in neutron-deficient Hg isotopes.

(c) The isomeric quadrupole moments in the Pb isotopes are also reproduced quantitatively, but the additional core deformation is very small. For the isotopes above $N = 114$, the experimental values are even slightly lower than the theoretical trend line, indicating that the core polarization saturates only below $N = 114$ for these neutron isomers. This is in agreement with the conclusions derived from the proton quadrupole moments in $Z > 82$ isotopes in figure 7, which also suggest a constant core polarization $\beta_2^{\text{core}} \sim 0.05$ below $N = 114$. The core deformation in these proton states in trans-lead nuclei is however significantly larger than in the neutron states (about factor 2) due to the additional proton–neutron interaction in the former. Furthermore, the proton intruder states in the Pb nuclei involving a 2p–2h proton core-excitation, are found to be rather deformed $\beta_2 \sim -0.16$ (see section 2.2.2), thus confirming experimentally that they belong to a different minimum of the potential energy surface of the Pb isotopes [52].

(d) The fact that the quadrupole moments in the Hg-chain all agree with a constant core deformation suggests that due to the open proton shell, a small constant core polarization sets in much faster than in the closed shell $Z = 82$ Pb nuclei.

2.2.4. Additivity of the E2-operator for configurations with protons and neutrons. If the particle–particle coupling between protons and neutrons is weak (= weak coupling limit) the wave function of a nuclear state can be expressed as the direct product of the proton and neutron part: $|(J_\pi \otimes J_\nu);\, Jm\rangle$. Starting from the fact that the quadrupole operator is a one-body operator, we can write:

$$Q_{\text{s}}(J) \equiv \langle J_\pi \otimes J_\nu);\, J, m = J | \boldsymbol{Q}_z(\pi) + \boldsymbol{Q}_z(\nu) | (J_\pi \otimes J_\nu);\, J, m = J \rangle \qquad (2.12)$$

This quadrupole moment can be written as a function of the respective proton and neutron quadrupole moments $Q_{\text{s}}(J_\pi)$ and $Q_{\text{s}}(J_\nu)$ using angular momentum coupling rules and tensor reduction rules [24]:

$$\begin{aligned} Q_{\text{s}}(J) = {} & \begin{pmatrix} J & 2 & J \\ -J & 0 & J \end{pmatrix} (-1)^{J_\pi + J_\nu + J} (2J+1) \\ & \times \left[\begin{Bmatrix} J_\pi & J & J_\nu \\ J & J_\pi & 2 \end{Bmatrix} \frac{Q_{\text{s}}(J_\pi)}{\begin{pmatrix} J_\pi & 2 & J_\pi \\ -J_\pi & 0 & J_\pi \end{pmatrix}} + \begin{Bmatrix} J_\nu & J & J_\pi \\ J & J_\nu & 2 \end{Bmatrix} \frac{Q_{\text{s}}(J_\nu)}{\begin{pmatrix} J_\nu & 2 & J_\nu \\ -J_\nu & 0 & J_\nu \end{pmatrix}} \right] \end{aligned} \qquad (2.13)$$

This rule is obviously also valid for two identical particles in different orbits coupling to a total spin J.

For high-spin isomers near closed shells, where the total spin is obtained by a full alignment of the single particle spins of valence protons and neutrons, the isomeric state can be described with a nearly pure configuration. In such case, the additivity rule is usually a good approximation to calculate the experimental quadrupole moments. Examples for isomeric states in the In and Sn isotopes can be found in [56]. Here, we present the comparison of calculated and experimental moments of high-spin isomers in the trans-lead region, including neutron core-excited states (table 3 and figure 9). The data are taken from [1, 43, 44]. The single particle quadrupole moments that are used in the calculations were obtained using (2.7), with a neutron dependent proton effective charge $e_\pi^{\text{emp}}(N)$ from table 2 and a constant neutron effective charge $e_\nu^{\text{emp}} = 0.95e$.

The experimental At quadrupole moments are well reproduced with the renormalized effective charges and assuming pure configurations. Notice that configurations including only the $\pi 1\text{h}_{9/2}$ orbit have a smaller quadrupole moment than configurations with, respectively, 1 and 2 protons in the $\pi 1\text{i}_{13/2}$ orbit. The core-excited quadrupole moments in the astatine

Table 3. Empirical quadrupole moments calculated for the pure configurations from [43, 44, 59]. The neutron core-excited isomers are indicated in bold.

Isotope	N	Spin	Decoupling into $Q_{\text{s.p.}}$	Q_{exp} (efm^2)	Q_{emp} (efm^2)
^{208}At	123	16^-	$1.29Q(\pi h_{9/2}) + 0.97Q(\pi i_{13/2}) - 0.02Q(\nu f_{5/2}^{-1})$	−169(25)	−166
^{209}At	124	$21/2^-$	$1.17Q(\pi h_{9/2})$	−78(8)	−69
		$29/2^+$	$1.33Q(\pi h_{9/2}) + Q(\pi i_{13/2})$	−150(15)	−153
^{210}At	125	11^+	$1.17Q(\pi h_{9/2})$	−65(8)	−60
		15^-	$1.33Q(\pi h_{9/2}) + Q(\pi i_{13/2})$	−122(12)	−134
		19^+	$\mathbf{1.33}Q(\pi \mathbf{h_{9/2}}) + Q(\pi \mathbf{i_{13/2}}) + Q(\nu \mathbf{g_{9/2}})$	**−220(25)**	**−182**
^{211}At	126	$21/2^-$	$1.17Q(\pi h_{9/2})$	−53(5)	−51
		$29/2^+$	$1.33Q(\pi h_{9/2}) + Q(\pi i_{13/2})$	−101(19)	−114
		$39/2^-$	$\mathbf{1.29}Q(\pi \mathbf{h_{9/2}}) + \mathbf{0.97}Q(\pi \mathbf{i_{13/2}}) + Q(\nu \mathbf{g_{9/2}})$	**−191(25)**	**−163**
^{208}Rn	122	8^+	$0.44Q(\pi h_{9/2})$	−41(5)	−32
^{210}Rn	124	8^+	$0.44Q(\pi h_{9/2})$	−32(4)	−26
		17^-	$1.17Q(\pi h_{9/2}) + Q(\pi i_{13/2})$	−89(10)	−144
^{211}Rn	125	$17/2^-$	$0.44Q(\pi h_{9/2})$	−19(2)	−23
		$63/2^+$	$\mathbf{1.17}Q(\pi \mathbf{h_{9/2}}) + Q(\pi \mathbf{i_{13/2}}) + Q(\nu \mathbf{f_{5/2}^{-1}}) + Q(\nu \mathbf{g_{9/2}}) + Q(\nu \mathbf{j_{15/2}})$	**−160(22)**	**−188**
^{212}Rn	126	8^+	$0.44Q(\pi h_{9/2})$	−18(2)	−19
^{211}Fr	124	$29/2^+$	$0.44Q(\pi h_{9/2}) + Q(\pi i_{13/2})$	−107(18)	−100
		$45/2^-$	$1.17Q(\pi h_{9/2}) + 1.54Q(\pi i_{13/2})$	−198(56)	−184
^{212}Fr	125	15^-	$0.44Q(\pi h_{9/2}) + Q(\pi i_{13/2})$	−84(13)	−88
		27^-	$\mathbf{1.17}Q(\pi \mathbf{h_{9/2}}) + \mathbf{1.54}Q(\pi \mathbf{i_{13/2}}) + Q(\nu \mathbf{g_{9/2}})$	**−174(33)**	**−213**
^{213}Fr	126	$29/2^+$	$0.44Q(\pi h_{9/2}) + Q(\pi i_{13/2})$	−70(7)	−74
		$65/2^-$	$\mathbf{1.17}Q(\pi \mathbf{h_{9/2}}) + \mathbf{1.54}Q(\pi \mathbf{i_{13/2}}) + Q(\nu \mathbf{g_{9/2}}) + Q(\nu \mathbf{i_{11/2}})$	**−219(53)**	**−242**

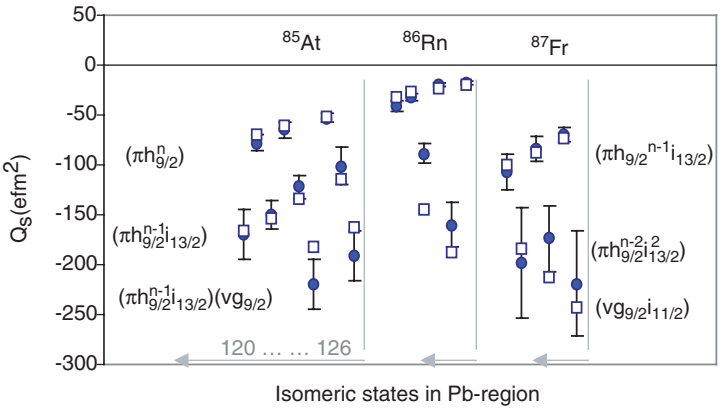

Figure 9. Experimental quadrupole moments (●) of high-spin isomeric states in At, Rn and Fr isotopes near $N = 126$ compared to empirical values (□) assuming pure configurations (see text for details).

isotopes are slightly underestimated. This might suggest that also the neutron effective charge needs to be corrected for the number of holes in the $\nu(3p_{1/2})^{-n}$ orbit. In ^{211}At the core-excited $39/2^-$ isomer involves a 1p-1h neutron excitation, leaving 1 hole in the $N = 126$ shell, while in ^{210}At the 19^+ isomeric 1p-1h core-excited state leaves 2 holes in $N = 126$. Using the same relative neutron effective charges as for the protons (Table 2), the calculated moments are respectively, $Q(19^+) = -196$ efm^2 and $Q(39/2^-) = -171$ efm^2, in better agreement with the experimental values.

In the Fr isotopes, a good agreement is found for all isomeric states. The experimental values for the isomeric states in ^{211}Fr measured with the time differential perturbed angular distribution (TDPAD) method [57] are in slightly better agreement with the calculated values than the results obtained with the level mixing spectroscopy (LEMS) technique [58]. The good agreement with the calculated values supports the idea that high-spin isomeric states are well described with rather pure configurations, and that the assumed configurations are the proper ones. If in the core-excited isomeric states a renormalized neutron effective charge is used, similar to that described for the At high-spin isomers, the calculated quadrupole moments slightly overestimate the experimental values.

In the Rn isotopes all experimental results are reproduced by the calculations, except for the (normal) high-spin isomer in ^{210}Rn. The empirical quadrupole moment for a pure $[\pi(\mathrm{h}_{9/2})^3\mathrm{i}_{13/2}\,\nu(\mathrm{p}_{1/2})^{-2}]_{17^-}$ configuration overestimates the experimental value. Because all other quadrupole moments in this region are very well reproduced, including the core-excited ones, this is a strong indication that either the experimental value is wrong or the suggested configuration is not pure. Configuration mixing typically occurs if several configurations can lead to a state with the same spin and similar excitation energy (within $\sim$1 MeV) [24]. In [59], the quadrupole moment was calculated for several configurations leading to the $I^\pi = 17^-$ state, resulting all in similar values. This seems to suggest that configuration mixing cannot explain the deviation between the experimental and calculated value.

2.2.5. Breakdown of the E2-additivity for strongly interacting protons and neutrons. As mentioned before, only in the weak coupling limit it is possible to describe the empirical quadrupole moment for a composed proton–neutron state as a linear combination of the respective proton- and neutron-quadrupole moments. If the experimental quadrupole moment of a composed state does not agree with the empirical additivity value, it can be an indication that there is a strong interaction between the protons and the neutrons. In that case, the wave function cannot be decoupled into its proton and neutron part only [60].

An illustration of the breakdown of the E2-additivity was suggested recently for the band head of an M1 rotational band in ^{196}Pb. The intra-band decay in these rotational bands does not occur via E2-transitions (as seen in bands built on deformed and super-deformed nuclear states), but via M1 transitions (suggesting that a magnetic dipole is at the origin of the rotation). Many properties of rotational M1-bands in the neutron-deficient Pb isotopes have been described by the 'shears' mechanism: the bands are built on a state formed by the perpendicular coupling between an intruder proton configuration and a normal neutron configuration [61]. Due to this perpendicular coupling, the dipole moment of this state is not parallel to its total spin. This allows for a new quantum-mechanical rotation: the rotation of a magnetic dipole, resulting in a 'magnetic rotational band', described by the tilted axis cranking (TAC) model [62]. In many cases, both the proton and neutron configurations involved in these rotational bands are occurring as isomeric states in these nuclei. Examples are the $\pi(1\mathrm{h}_{9/2}1\mathrm{i}_{13/2})_{11^-}$ intruder isomers coupling to $\nu(1\mathrm{i}_{13/2}^{-n})$ 12^+ or $13/2^+$ isomers, to form a band head with spins ranging from 15 to $18\hbar$ [61, 63]. Because of the short lifetime of the band heads (although only a few band head lifetimes have been reported), it is difficult to measure their nuclear moments. By measuring the magnetic and quadrupole moments of the involved isomeric states, the nuclear moments of the band heads might be deduced using the additivity rules for nuclear moments, provided the coupling between the proton particles and neutron holes is not too strong. One direct measurement of a band head magnetic moment has been reported so far: for the ^{193}Pb $29/2^-$ band head a g factor $g_{\mathrm{exp}}(29/2^-) = 0.68(3)$ is found to be in agreement with the g factor calculated with the additivity rule (2.4) for a pure $[\pi(1\mathrm{h}_{9/2}1\mathrm{i}_{13/2})_{11^-} \otimes \nu(1\mathrm{i}_{13/2}^{-1})]_{29/2-}$ configuration: $g_{\mathrm{add}} = 0.71(4)$ [64]. This good agreement was used as an argument to prove

that the configuration of this band head is indeed a perpendicular coupling of the suggested proton and neutron states. To measure the quadrupole moment of this band head is much more difficult, due to the very short lifetime ($T_{1/2} = 9$ ns). Recently, the quadrupole moment of the 11^- intruder state was measured in ^{196}Pb $Q_{\rm exp}(11^-) = -341(66)\,{\rm efm}^2$ [34]. The additivity rule was applied to calculate the quadrupole moment of the M1 band head in this isotope, suggested to have a $[\pi(1h_{9/2}1i_{13/2})_{11^-} \otimes \nu(1i_{13/2}^{-2})]_{16-}$ configuration. A very small quadrupole moment was deduced $Q_{\rm add}(16^-) = -32\,{\rm efm}^2$. This value is not in agreement with the quadrupole moment predicted in the TAC model, which predicts $Q_{\rm TAC}(16^-) = -120\,{\rm efm}^2$ and a deformation $\beta_2^{\rm TAC} \sim -0.13$. Note that the TAC model predicts a similar deformation for the intruder state and for the magnetic rotational band head and that the intruder state deformation is in reasonable agreement with the experimental value $\beta_2^{\rm exp}(11^-) = -0.16(3)$ [34].

It remains to be proven experimentally whether the additivity rule for nuclear quadrupole moments is valid in these nuclei or whether the TAC predictions for the band head quadrupole moment are correct. A breakdown in the additivity of the E2 operator for these M1 band heads could be initiated by a strong interaction between the proton particles and the neutron holes. On the other hand, the additivity of the M1 operator seems to persist for these states.

3. Production methods for exotic radioactive nuclei and the implications to moment measurements

When looking into the 'table of nuclear moments' published in 1989 by Raghavan [1] it is striking that nearly 60% of the measured nuclear moments are for ground states or isomeric states in nuclei on the neutron-deficient side of the valley of stability and 30% of the measured values are for stable nuclei. The fact that till 1989, very few measurements had been performed on neutron-rich nuclei is due to the lack of methods to produce and separate these neutron-rich nuclei. Furthermore, even if the nuclei could be produced, the study of their static moments requires in many cases the need for a spin-oriented nuclear ensemble. In this section, we will discuss how the methods for producing a spin-oriented ensemble of radioactive nuclei are strongly influenced by their production method.

In recent years, significant progress has been made in the production and selection of nuclei lying at the boundary of the nuclear chart [65], both towards the proton as well as to the neutron drip-line. The research on the properties of exotic nuclei, in which the study of nuclear moments has its own particular role, has grown to its full potential since several radioactive ion beam (RIB) facilities are now operational and are producing fascinating results. Furthermore, innovative R&D programs in Europe [66], North America [67] and Japan [68] are being pursued in order to prepare the second generation of RIB facilities.

Two types of RIB facilities can be distinguished, allowing production of pure beams of radioactive nuclei in a whole range of energies (from millielectronvolt to gigaelectronvolt) [69]: one is based on the ISOL method of production and mass separation, the other on the IF method of separating the high-energetic recoiling reaction products of interest using recoil spectrometers behind the target. The IF method for producing radioactive beams can be applied in several energy regimes, from around the coulomb barrier ($\sim$5 MeV u^{-1}) using inverse fusion–evaporation reactions and up to very high energies using projectile-fragmentation reactions (50–500 MeV u^{-1}).

Of course many of the moment measurements on radioactive nuclei are also still carried out directly around the target station, without a preceding selection procedure (these are called 'in-beam' experiments). This is required, e.g. if one is interested in studying properties of extremely short-lived excited states. In this case, the radioactive nuclei are produced and

stopped in (or immediately after) the target and all the radiation emitted at the target position is seen by the surrounding detectors. It is obvious that in this case, the study of very exotic nuclei will require advanced detection methods in order to extract the small amount of useful decays out of the large flux of radiation coming from all produced radioactive species. Also in this field, an important international effort has resulted in building large detectors arrays (including γ, β and particle detection). Examples are the EUROBALL array in Europe [70] and the GAMMASPHERE in the USA [71]. A second generation of γ arrays, based on the tracking of the γ-ray incident position in the detector crystal [72, 73] is now in preparation and will enhance the possibilities of in-beam experiments. Another new achievement from the last couple of years is the possibility to make reactions with post-accelerated radioactive beams to produce short-lived activity, e.g. excited states in the radioactive species via coulomb excitation.

In this paper, we will briefly explain how the production and selection methods for exotic radioactive nuclei are closely related to the type of experimental techniques that can be applied for the study of their nuclear moments, in the ground state or in some isomeric exited state.

3.1. In-beam production methods for nuclear moment studies

Most of the high-spin isomeric states for which nuclear moments have been investigated until recently, were produced in a fusion–evaporation reaction of a stable beam (accelerated to $\sim$5 MeV u^{-1}) with a stable target. In such a reaction, the projectile nucleus fuses with a target nucleus to form a new compound nucleus that lies close to the valley of stability. The compound nucleus is produced in a highly excited state and it will reduce its energy first by the evaporation of a few particles (mainly neutrons). Consequently mainly neutron-deficient radioactive nuclei are produced. These residual nuclei decay first via emission of statistical γ rays until the yrast line is reached and after that, they decay via discrete γ transitions along the yrast line towards the ground state [74, 75]. In many of these nuclei, isomeric states occur along this yrast line, so this production method is ideally suited for the study of high-spin isomeric states. Isomeric states with angular momentum up to 35$\hbar$ and more have been produced in such reactions.

A further important advantage of the fusion–evaporation production method, related to the study of nuclear moments, is the fact that the spins of the produced isomeric states have a preferred orientation: the isomeric spins are oriented preferentially perpendicular to the beam axis, thus giving rise to a large oblate aligned ensemble of nuclear spins with the alignment axis along the beam line [74]. More details on the different types of nuclear orientation are discussed in next section.

In coulomb excitation reactions, where either the target or the projectile nucleus gets excited by the coulomb field of its partner, the excited nuclear states will also exhibit a very high amount of spin-orientation [75, 76] This production method is in particular useful for the investigation of moments in well-deformed nuclei, as the members of a ground state rotational band are easily excited in such a reaction [77].

3.2. ISOL techniques for radioactive beam production

3.2.1. Low-energy beams (<100 keV). In the ISOL facilities, the radioactive nuclei are produced with some nuclear reaction after which they are collected in a solid (thick target), in a liquid or in a gas (at high or low pressure). If this collection process leads to neutralization of the atoms, they are re-ionized, e.g. by surface ionization, by resonant laser ionization or in an electron cyclotron resonance (ECR) ion source. If not neutralized, the ions are extracted (e.g. via a He jet) out of the collection chamber and in all cases the ions are accelerated electrostatically to about 40–60 keV and injected into a mass separator. In this way, a relatively pure

beam of one particular mass can be obtained with a rather good beam quality (small longitudinal and transverse energy spread). Over the past years, a large variety of ISOL techniques has been developed and new developments are still going on. A good overview on these developments can be found in [78]. The oldest (but still one of the best performing) of this type of facilities is ISOLDE CERN [79]. At this facility the radioactive nuclei are produced by a high-energy proton beam (1–1.4 GeV) inducing a fragmentation reaction of a heavy target element (Ta, U, etc). In this way, almost all nuclei in the nuclear chart, including the very exotic ones, can be produced. However, one of the problems is to get the radioactive nuclei out of the very thick target (thickness several $\mathrm{g\,cm^{-2}}$) by diffusion. Heating the target to very high temperatures enhances the diffusion process, but still only non-refractory elements diffuse out of the thick target [80]. Only radioactive species with lifetimes of the order of several milliseconds are obtained by this production process. Shorter lived activity simply dies in the target-ion source system and never reaches the experimental end-station. A solution to this is to use another (faster) type of reaction mechanism for the production of the radioactive nuclei of refractory and short-lived isotopes, such as a fusion–evaporation reaction or reaction induced fission on a thin target and then catching the recoiling radioactive nuclei in an ion-guide [81, 82]. This is called the ion-guide isotope separation on-line (IGISOL) method. The beam quality from the IGISOL production scheme is inferior to that from ISOL ion source methods. Recent developments related to beam-cooling methods have largely improved the IGISOL beam quality to energy resolutions below 1 keV [83–85]. That is of importance for the application of collinear laser spectroscopy methods to study the moments and radii of these beams [86].

Another problem related to the ISOL method that had to be solved is related to the mass separation process, which allows only an isobaric separation. That means that the study of the most exotic nuclei was for some time excluded because of the production and selection of nuclei with a similar mass but much less exotic, thus being much more abundant. This problem could be solved by the development of a 'laser ion source' in which atoms of one particular element are resonantly ionized by a laser beam [87–89]. This technique is highly element selective, and coupled with a high-resolution mass separator it produces a pure beam of exotic nuclei with good ion-optical qualities.

3.2.2. Post-accelerated ISOL beams. Once the ISOL production method had been fully explored and used for the study of exotic radioactive beams at the kiloelectronvolt energy level, it was realized that these radioactive beams could be re-accelerated. High-intensity post-accelerated radioactive beams would allow us, e.g. to investigate the properties of these exotic nuclei via transfer or coulomb excitation reactions. Such high-energetic radioactive beams were already available from the IF projectile-fragmentation facilities (see next section and e.g. the proceedings of the first and second Radioactive Ion Beam conferences [3, 4]). However, the radioactive beams from these IF facilities have a few drawbacks, such as the very poor beam quality (in terms of energy resolution and beam spot) and the very high-energy (typically 40–300 $\mathrm{MeV\,u^{-1}}$), which is suited only for particular types of experiments. For reaction studies around the coulomb barrier (and below) or for experiments of astrophysical interest, these beams are not well suited. Radioactive beams with a good ion-optical quality and energy resolution and with energies between 1 and 5 $\mathrm{MeV\,u^{-1}}$, which could be obtained by re-accelerating the radioactive beams obtained from the ISOL facility, are ideally suited for experiments of astrophysical and nuclear structure interest.

The first post-accelerated radioactive beam was produced by the Centre de Recherche Cyclotron (CRC) at the university of Louvain-la-Neuve, Belgium, in 1989 [5]. Since then, the RIB project of the CRC has produced, for more than a decade, post-accelerated ISOL beams at

energies of about 5 MeV u^{-1} by coupling two cyclotrons (a list of accelerated RIBs with their respective intensities is available on www.cyc.ucl.ac.be). The potential for nuclear astrophysics studies has recently been increased by the installation of a new cyclotron ($k = 44$) [6] providing radioactive beams with energies around 1–2 MeV u^{-1}. In 2001, two other European facilities came into operation. The SPIRAL project couples a new cyclotron ($k = 265$) to the existing cyclotrons of GANIL, Caen, France and produced in 2001 its first post-accelerated beam (1.67 s ^{18}Ne), which was directly used in successful experiments [7]. The REX-ISOLDE project makes use of the multitude of low-energy radioactive beams of ISOLDE, CERN, Geneva, Switzerland and post-accelerates them by the combination of a Penning trap, where the ions are stored and cooled, an electron beam ion source (EBIS) for charge-breeding, and a linear accelelator (LINAC) accelerating the radioactive ions to an energy between 0.8 and 2.2 MeV u^{-1} [8]. Also here the post-accelerated beams (e.g. neutron-rich Li, Na and Mg isotopes) have successfully been used for nuclear physics experiments. An upgrade of the accelerator to reach energies up to 3.5 MeV u^{-1} is in progress.

In North America, the Holifield radioactive ion beam facility (HRIBF) at Oak Ridge National Laboratories, USA completed the first experiments in 1998 using ^{18}F beams, post-accelerated by a 25 MV Tandem. Since then other beams, both on the proton-rich as well as on the neutron-rich side, have been available for experiments [10]. The ISAC facility at TRIUMF, Vancouver, Canada started operation in 1998 as well and since then many experiments of nuclear and astrophysics interest have been performed with beams accelerated up to 1.5 MeV u^{-1}. Continuous development on the target-ion source system has led to a continuous increase of the primary beam on target from 1 to 40 μA (corresponding to a beam power of 20 kW). This development is of prime importance for the second generation of RIB facilities where megawatt beams are considered.

In fact in Europe, in North America and in Japan, plans for a second generation of RIB facilities are aiming to improve the general performances of the present-day facilities by several orders of magnitude. Modern accelerator technology will make it possible to deliver driver-beam intensities on the primary target which go far beyond the intensities achieved nowadays for the IF and ISOL techniques. But the new plans are not only based on a 'simple' increase of the intensity. New approaches are explored, such as the gas catcher technique, which combines the strong points of the IF and ISOL techniques [90]. By using a gas cell for stopping relativistic radioactive ions, purified by the IF technique, and injecting them in an ISOL system, radioactive ion beams of excellent ion-optical quality (superior to IF beams) can be obtained [91].

All ISOL-produced radioactive beams are obviously not spin-oriented and only elements with a sufficiently long lifetime (to survive the collection, re-ionization and mass selection process) can be produced (typically of the order of milliseconds and depending on each particular target-ion source combination). For precision nuclear moment measurements on these radioactive beams, using, e.g. β-NMR methods, it is important that methods to polarize these radioactive beams are developed. Several such techniques have been explored already (see section 4) and some of them have been applied very successfully. However, further research and development in this field is going on at this moment.

3.3. IF methods to produce beams of radioactive nuclei

Measuring nuclear moments of exotic short-lived nuclear states (half-lives of the order of 100 ns up to 100 ms) requires fast spin-orientation methods combined with fast exotic-beam production and selection methods. Because some nuclear reactions provide automatically a spin-oriented ensemble of exotic radioactive nuclei, it is obvious that one of the most elegant

ways to investigate the moments of rarely-produced nuclei is via the IF selection method, while trying to maintain the spin-orientation during the selection process.

In-flight separation of the exotic nuclei is possible if the reaction products have sufficient energy to recoil out of the production target. That happens if the primary beam that induces a nuclear reaction has a sufficiently high-energy and/or the mass of the projectile is larger than the mass of the target nuclei. The variety of reaction products from such a reaction is usually very high (similar as in the ISOL scheme) and a method is needed to select the exotic nucleus of interest out of all the unwanted other nuclei that are produced. Because of the high recoil velocity of the reaction products and the fact that the recoil happens in the forward direction, it is clear that IF mass separation is ideally suited to separate the nuclei of interest in a fast way from the primary beam and from the other reaction products.

One can distinguish two energy regimes in which IF mass separation is applied.

3.3.1. IF separation around the coulomb barrier. In the range 5–10 MeV u^{-1} one uses, e.g. an inverse kinematics fusion–evaporation reaction to produce mainly exotic nuclei on the neutron-deficient side of the nuclear chart, approaching the proton drip-lines. Different types of mass spectrometers can be used to separate the nuclei of interest from the beam and from some other reaction products, e.g. using a dipole-based recoil separator CAMEL at Legnaro National Laboratory, Legnaro, Italy [92], a combined magnetic and electrostatic mass spectrometer such as FMA in Argonne National Laboratory, USA [93], or a gas-filled recoil separator RITU at Jyväskylä, Finland [94].

The advantage of using these devices as compared to in-beam experiments is of course the possibility to perform low-background experiments on exotic nuclei and isomeric states at the focal plane of the recoil spectrometer [95]. Another option is to put a high-efficiency γ array around the target position in front of the recoil spectrometer, and to request a coincidence condition between the detected γ-ray and a particular recoiling ion identified behind the recoil spectrometer [96]. This recoil tagging method as well as the recoil decay tagging [97] technique, allows production of γ spectra that contain only the radiation from the nucleus of interest. These methods are nowadays being further improved by developing dedicated particle and γ detection arrays for the focal plane and the target position. Such developments are continuing at the stable beam facilities and they are also being built for the new radioactive beam facilities where they are indispensable due to the very exotic reactions that take place with radioactive beams (e.g. the VAMOS spectrometer [98] has been coupled to the EXOGAM array [99] at the SPIRAL radioactive beam facility of GANIL, Caen, France [100]).

There are two limitations that make it difficult to perform nuclear moment measurements on nuclei at the focal plane of a recoil spectrometer, although such measurements would highly benefit from the reduced background conditions. The first one is related to the rate of isomers (or nuclear ground states) reaching the focal plane, the second one is related to the fact that for moment measurements on nuclear states with typical lifetimes of 10^{-7}–1 s, a spin-oriented ensemble is required. In fact, there is a kind of optimal condition expressed in terms of these two parameters, which dictates whether or not a moment measurement is possible: if the detected decay rate (s^{-1}) multiplied by the detected change in anisotropy squared is of the order of 0.1–1 s^{-1}. The required radioactive beam rate behind the recoil separator will thus strongly depend on the efficiency of the detection system used (β or γ detection) as well as on the amount of spin-orientation that is present in the recoil-separated ensemble.

The problem related to the spin-orientation is the fact that the recoiling nuclei are not fully stripped when they recoil out of the target [101]. In these free atoms recoiling in vacuum, the electron spin J couples to the nuclear spin I to form a total atomic spin F (known as the atomic hyperfine interaction) [102]. Due to this interaction, the randomly oriented electron spins

will reduce the nuclear spin-orientation to some hard-core value [103]. A further reduction of the atomic spin-orientation (and thus of the nuclear spin-orientation) is established by the interaction of the strong electron dipole (10^3 times stronger than the nuclear dipole) with the magnetic dipole fields in the mass separator. So, after recoil mass separation in vacuum, the initial spin-orientation induced by the fusion–evaporation reaction is likely to be completely washed out if the selected nuclei are not naked. In such a case, nuclear spin-orientation should be introduced after the selection procedure in a fast and universal way, which might be done e.g. by the beam multi-foil interaction method (see next section).

Another solution might exist, that is if the recoiling atoms are produced (partly) in a noble gas charge state (thus with $J = 0$) and if this charge state of the recoiling nuclei can be separated from the other charge states by the recoil spectrometer. In that case, the atomic spin equals the nuclear spin, and so only rotation of the nuclear spins in the dipoles of the mass separator needs to be taken into account. If the ions all follow a trajectory in which they are submitted to the same magnetic field strength, then the Larmor precession frequency is the same for all these nuclei and thus at the focal plane an ensemble with some (reduced) orientation will be observed, with the orientation axis rotated with respect to the beam direction [104]. In fact, experiments on noble gas charge states selected after in-vacuum recoil separation has been performed [105] and indeed a significant amount of the orientation was found in the selected isomeric states behind the recoil spectrometer at Rochester. It is clear that in some well-chosen cases it can be a unique way to measure the moments of very neutron-deficient isomeric states far from stability. The spin-orientation which remains is not very large, but in any case similar to the orientation after beam multi-foil interaction or after IF projectile fragmentation (see section 4).

Notice that in combination with a gas-filled recoil separator (such as RITU at Jyväskylä), which is especially suited for the study of heavy elements [106], it is at this moment not clear whether the spin-orientation can be maintained during flight. Studies of the preservation of spin-orientation in the case of recoils in a gas were performed several decades ago [107, 108], but never for such long flight times as in a recoil separator. A detailed study on the subject, in combination with the interactions occurring in a mass separator would be required to investigate this option. It could be a unique way to study the moments of the heaviest elements, which are not accessible by other means.

3.3.2. IF separation after intermediate and high-energy projectile-fragmentation reactions. The most common way to produce exotic radioactive nuclei with extreme proton/neutron ratios is the projectile-fragmentation reaction. At high beam energies ($>100\,\mathrm{MeV\,u^{-1}}$) a peripheral interaction between a heavy projectile and a target nucleus induces the breakup of the fast projectile into a variety of secondary ions lighter than the beam. By the fragmentation of a stable neutron-rich nucleus (the heaviest being ^{238}U) one can produce extremely neutron-rich nuclei for almost all elements, and similarly nuclei at the proton drip-line are reached by fragmentation of a very proton-rich stable isotope. The cross sections for projectile fragmentation are nowadays rather well reproduced [109] and obviously drop drastically when removing/adding more and more neutrons when going towards the drip-lines (typically an order of magnitude per neutron). Another efficient way of producing very neutron-rich nuclei for particular elements is by projectile fission. Recently, more than 100 new isotopes were identified in just a few days experiment using the projectile fission process at the fragment recoil separator (FRS) at GSI-Darmstadt [110].

At intermediate beam energies (40–$80\,\mathrm{MeV\,u^{-1}}$) the projectile-fragmentation process competes with other reactions such as the transfer reaction, the nucleon pick-up reaction, etc. The calculation of the reaction cross section is more complex and somewhat less reliable (regarding absolute numbers). However, a very user friendly and powerful tool for estimating

secondary beams rates produced and selected at several IF projectile-fragmentation facilities worldwide is the LISE code [111].

At these IF projectile-fragmentation facilities, the secondary beam is purified using an achromatic (or doubly achromatic) high-resolution mass separator, such as LISE at GANIL, Caen, France [112], the A1200 at the NSCL, Michigan, USA [113] which has recently been upgraded to the A1900, the FRS at GSI Darmstadt, Germany [114] and RIPS at RIKEN, Tokyo, Japan [115]. Extremely pure beams of exotic radioactive nuclei can be obtained at rather high intensities, especially if further purification is performed with a velocity filter, such as the WIEN-filter at GANIL [116]. For some applications one prefers a cocktail of exotic radioactive nuclei at rather low intensity, and such beams can easily be obtained, depending on the settings and the properties of the isotope selection devices.

Some important aspects related to radioactive beams produced by IF projectile-fragmentation methods will have a direct impact on the experiments that can be performed with them. These radioactive beams have a high-energy (40 up to several 100 MeV u^{-1}) with a poor energy resolution, the beam quality is rather poor: a large beam spot at the focal point of $(1 \times 2)\,cm^2$ at intermediate energies and at least $(5 \times 5)\,cm^2$ at high beam energies.

An advantage of fragmentation beams is that they are inherently made spin-oriented by the fragmentation reaction itself (see section 4), and because most (at least light mass) fragment beams are being fully stripped, the reaction-induced spin-orientation is maintained up to the focal point where the beam can be implanted for nuclear moment studies.

4. Spin-orientation of radioactive beams and exotic nuclei

4.1. Definitions: spin-alignment and spin-polarization

An ensemble of nuclei is spin-oriented if the nuclear spins have a preferential direction in space. By defining a Z-axis, one can describe the spin-orientation with respect to this axis by the probability p_m that the nuclear spin has a projection $|m\rangle$ onto this axis. If the Z-axis is an axial symmetry-axis of the oriented ensemble (called the Z_{OR} axis, figure 10), then the orientation is fully determined by these probabilities p_m. For a non-axially symmetric oriented ensemble, the density matrix formalism has to be used to describe the orientation:

$$\rho_{mm'} = \langle m|\rho|m'\rangle$$

The diagonal elements $\rho_{m,m} = p_m$ describe the population of the different spin-projections and the non-diagonal elements describe the coherence between the different m-states. This

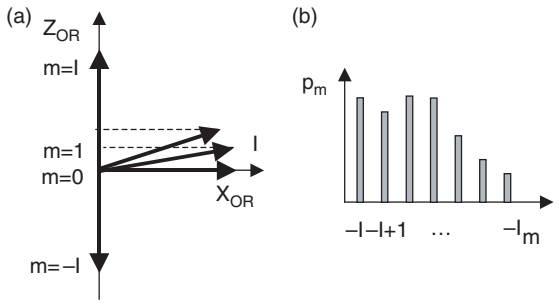

Figure 10. (*a*) The projection of the nuclear spin I on a chosen Z-axis is defined as m. (*b*) If the spin ensemble has an axial symmetric orientation around the Z_{OR} axis, then the orientation is fully described by the probabilities p_m of occupying the m-quantum states.

density matrix is related to the density tensor ρ_k^n [75]:

$$\rho_k^n = \sqrt{2k+1}\sum_m (-1)^{I+m} \begin{pmatrix} I & I & k \\ m & -m' & n \end{pmatrix} \langle m|\rho|m'\rangle \tag{4.1}$$

and to the orientation tensor $B_k^n = \sqrt{2I+1}\rho_k^{n*}$.

In the angular distribution of the radiation emitted from an oriented ensemble, the spin-orientation will always be described by the orientation tensor, because it allows the distribution function to be easily transformed from one axis-system to another by rotation over the Euler angles. However, when speaking about the amount of orientation, a different terminology tends to be used, depending on the type of orientation. The relation between the orientation tensor components and the definition of 'alignment' and 'polarization' is explained hereafter.

4.1.1. Alignment A of nuclear spins. An ensemble of spins is called aligned if it has an axially symmetric distribution of the spins and if there exists reflection symmetry with respect to a plane perpendicular to the axial symmetry-axis. This means $p_m = p_{-m}$ (figure 11). The nuclear alignment is proportional to $\sum_m (3m^2 - I(I+1))p_m$ and is directly related to the second-order orientation tensor [27, 75]:

$$\begin{aligned} B_2^0 &= \sqrt{2I+1}\sqrt{5}\sum_m (-1)^{I+m} \begin{pmatrix} I & I & 2 \\ -m & m & 0 \end{pmatrix} p_m \\ &= \frac{\sqrt{5}}{\sqrt{I(I+1)(2I+3)(2I-1)}} \sum_m [3m^2 - I(I+1)]p_m \end{aligned} \tag{4.2}$$

The normalized alignment A is defined as:

$$A \equiv \frac{\sum_m \alpha_2(m)p_m}{|\alpha_2(\max)|} = \frac{\sum_m (3m^2 - I(I+1))p_m}{\alpha_2(\max)|} \tag{4.3}$$

with $\alpha_2(m) = 3m^2 - I(I+1)$. The normalization value $\alpha_2(\max)$ depends on whether oblate or prolate alignment occurs.

For maximum oblate alignment $A = -1$, all spins are oriented perpendicular to the Z-axis, i.e. $m = 0$ or $\pm\frac{1}{2}$. Then $\alpha_2(\max)$ is:

$$\begin{aligned} &|\alpha_2(m=0)| = I(I+1) && \text{for integer spin} \\ &|\alpha_2(m=\pm\tfrac{1}{2})| = I(I+1) - \tfrac{3}{4} && \text{for half integer spin} \end{aligned}$$

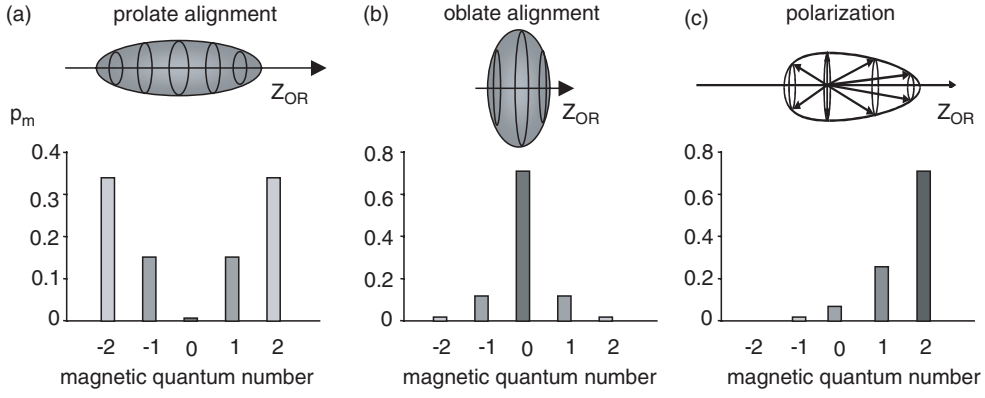

Figure 11. Different types of axial symmetric orientation.

For maximum prolate alignment $A = +1$, all spins are pointing along the Z-axis so $m = I$, and $\alpha_2(\max)$ is:

$$|\alpha_2(m = I)| = I(2I - 1) \qquad \text{for any spin}$$

The alignment is then related to the second-order orientation tensor as follows:

$$B_2^0 = \frac{\sqrt{5}|\alpha_2(\max)|}{\sqrt{I(I+1)(2I+3)(2I-1)}} A \tag{4.4}$$

Note that an aligned ensemble is described by the orientation tensors of even rank k: B_2^0, B_4^0, etc. Odd tensor ranks are zero. For some cases one can limit to the lowest order only, and thus describe the orientation by one parameter A. This has however to be studied case-by-case.

4.1.2. Polarization P of nuclear spins. An ensemble of nuclei is polarized if the up/down symmetry along the axial symmetry-axis is broken: $p_m \neq p_{-m}$. The nuclear polarization is proportional to $\sum_m m p_m$ and is related to the orientation tensor of first order:

$$\begin{aligned} B_1^0 &= \sqrt{2I+1}\sqrt{3}\sum_m (-1)^{I+m} \begin{pmatrix} I & I & 1 \\ -m & m & 0 \end{pmatrix} p_m \\ &= \frac{-\sqrt{3}}{\sqrt{I(I+1)}} \sum_m m p_m \end{aligned} \tag{4.5}$$

The normalized polarization is defined such that $P = +1$ if all spins are parallel to the Z-axis, and $P = -1$ if all spins are anti-parallel to the Z-axis:

$$P = \frac{\sum_m m p_m}{I} \tag{4.6}$$

and consequently the relation between the polarization and first-order orientation tensor is:

$$B_1^0 = \frac{-\sqrt{3}I}{(I+1)} P \tag{4.7}$$

In general, a polarized ensemble is described by both even and odd tensor components, because a purely polarized ensemble is rather rare. However, in the angular distribution of polarized radiation, e.g. if one studies the asymmetry in the β decay (section 5.1), one will often take into account the first-order density tensor only.

4.2. Methods to orient nuclei and application to radioactive nuclear beams

We give a few examples of methods that can be used to orient radioactive nuclei. Details on these techniques can be found in the appropriate references. In this report, we mainly focus the discussion on the applicability of the methods, e.g. depending on the way the exotic nuclei are produced, but also depending on the nuclear lifetime and spin and on the chemical properties of the element.

4.2.1. Spin-orientation of ISOL beams. (a) A very efficient technique to obtain a radioactive beam of highly polarized nuclei for the alkaline and earth-alkaline elements is the optical pumping method [117, 118]. Nuclear polarization of typically 30–50% can be obtained by this technique which is based on the hyperfine interaction between the electron spin J and the nuclear spin I. The atomic electrons are polarized by the interaction of the atomic (or ionic) beam with a circularly polarized laser beam. By subsequent resonant excitation and decay of the electrons using resonant laser photons, the atom (ion) ends up in a highly polarized state after

several excitation/decay processes (from which the term 'optical pumping' is derived). This requires a collinear laser—atom (ion) beam in one particular charge state and the radioactive beam should have a very good energy resolution ($\sim$1 eV) in order to reduce doppler broadening of the resonant excitation lines. Therefore, the method is applied to the low-energy beams from an ISOL facility, either on the ion beam or after a charge exchange on the neutral atom beam. Some very successful experiments using this orientation technique are described in [119–122]. A narrow band continuous wave (CW) laser facility providing laser light in the complete visible and near UV spectral range could largely enhance the potential of this powerful method, by extending it to other elements. Furthermore, the application of ion-beam cooling methods, which are now in full development, could also enhance the possibilities of this method, in particular in combination with production methods giving radioactive beams of much less quality.

(b) One of the oldest methods to polarize nuclear spins is probably the low temperature nuclear orientation (LTNO) method [123]. It was used for the first time, in the experiment by Wu *et al* [124], who polarized the nuclear spins of a long-lived ^{60}Co source, to show the parity violation in β decay. The polarization is induced by implantation of the radioactive nuclei into a ferromagnetic host that is cooled down to extremely low-temperatures (mK) and which is submitted to an external magnetic field (0.01–0.1 T) needed to orient the internal hyperfine field (which can reach 10–100 T). Due to the large Zeeman splitting induced by the static magnetic fields and because of the low-temperature of the environment, the ensemble will evolve to a Boltzmann distribution of the nuclear spins over the non-degenerate m-quantum states. Thus, the nuclear spins are being polarized. The time to reach the Boltzmann equilibrium depends on the spin-lattice relaxation time of the impurity element in the host. These relaxation times are of the order of seconds or more, thus the radioactive nuclei which can be oriented with this method should have lifetimes of the order of seconds or higher. For the shorter lived radioactive nuclei (less than hours) an on-line implantation of the exotic radioactive nuclei is required. Several on-line LTNO facilities have been operational during the past decades at different ISOL facilities all over the world. Because the lifetime of the nuclei needs to be rather long, this technique is not suitable to orient nuclei very far from the stability line, where lifetimes become short. Typical amounts of polarization that can be obtained are of the order of 20–80%.

(c) A method which was only suggested theoretically, but might be explored in the future, is to produce a beam of polarized ions directly in the ion source system, more particularly by using the laser ion source with circularly polarized laser light [125]. With this technique, the resonantly excited and ionized ion beam is being polarized during its resonant excitation by using circularly polarized laser light. Nuclear polarizations of the order of 10–20% could be obtained. The main problems to be solved with this orientation procedure are related to the maintenance of the nuclear polarization during the mass separation process, up to the implantation point.

4.2.2. Spin-orientation of post-accelerated ISOL beams. A technique which has been applied successfully only in a few experiments but that can be applied for a wide range of radioactive nuclear beams produced by several types of reactions, is the tilted foil polarization method [126–131] (also called the beam foil polarization method). The basic idea is that when an atom (ion) passes through a thin foil that is tilted with respect to the beam direction, the electron spins of the ions leaving the foil become circularly polarized due to the atomic interactions at the foil surface. Once the beam is in the vacuum, the hyperfine interaction between the polarized atomic electron spin and the nuclear spin will induce a nuclear polarization. By placing several foils after each other at well-defined distances, the nuclear polarization can be further enhanced

and values up to 18% can be reached [131]. The nuclear polarization obtained is largest for high-spin states, increases with the number of foils and optimal polarization is reached for not too high beam velocities (around $E \sim 1\,\mathrm{MeV\,u^{-1}}$ a beam polarization of 15% has been observed [126]). Taking into account all these considerations, this method is best suited to polarize radioactive beams of nuclei at high-spin, e.g. isomeric states in exotic nuclei produced via fusion–evaporation and subsequently mass separated. The tilted foils polarization method produces a purely polarized beam: the alignment (tensor) component in the orientation is negligibly small. Therefore, only experiments which are sensitive to vector polarization (B_1^0) can be used in combination with this spin-orientation method. This is the case for experiments in which an asymmetry in the β decay is observed as well as for γ-LMR experiments or for TDPAD quadrupole moment measurements. In the case of β decay the radiation is parity-violating, while in the case of detection of γ anisotropies, the applied interactions need to be parity-violating. Notice that quadrupole moment measurements using polarized beams are sensitive to the sign of the quadrupole moment [131]. A g factor measurement on γ decaying isomeric states cannot be performed with a purely polarized ensemble of isomeric states. In exotic nuclei where mass separation will be a crucial issue, the tilted foil polarization method might be a good alternative to produce an oriented radioactive beam. Also for radioactive beams produced by the ISOL method, in particular for isomeric beams but also for some beams of nuclei having a relatively high-spin, the tilted foil orientation technique could be applicable. In this case, the post-acceleration of the radioactive beams is crucial in order to have sufficient energy to pass the multi-foil stack needed to enhance the nuclear polarization. Attempts using a high-voltage platform to accelerate the ISOL beams to $20\,\mathrm{keV\,u^{-1}}$ have been made [132] recently at ISOLDE. A polarization of only 0.7% was measured for ^{23}Mg ($T_{1/2} = 11.3\,\mathrm{s}$) nuclei implanted in a Pt host. Note however that in experiments involving spin-oriented nuclei, the maintenance of the nuclear spin-orientation after implantation is of at least the same importance as the production of the polarization itself. Effects such as radiation damage, the implantation behaviour or spin-lattice relaxation can easily reduce the produced spin-orientation once implanted into the crystal. This was recently demonstrated in a measurement of spin-polarized fragment beams [133]. Therefore, care has to be taken about these effects when preparing an experiment with spin-oriented beams.

4.2.3. Spin-oriented nuclei from reactions with polarized beams. The radioactive nuclei that are produced in nuclear reactions with beams of polarized electrons, deuterons, neutrons, tritons, are showing a high amount of spin-polarization [134–136]. However, the radioisotopes that are polarized by this manner, using reactions on stable reaction targets, occur near the valley of stability only.

4.2.4. Reaction-induced spin-orientation in fusion–evaporation, transfer, projectile fragmentation and fission reactions. The easiest and fastest way to get a spin-oriented ensemble of radioactive nuclei, is via the spin-orientation produced during the production reaction itself. This is in particular important for the study of very short-lived nuclear (excited) states.

- Isomers produced in a fusion–evaporation reaction [74, 137] are highly spin-oriented. It has been shown that for all (heavy ion, xn) and (alfa, xn) reactions, the spin-alignment of the isomers can be described by a Gaussian distribution function

$$p_m = \frac{\mathrm{e}^{-m^2/2\sigma^2}}{\sum'_m \mathrm{e}^{-m'^2/2\sigma^2}}$$

with a typical width $\sigma/I = 0.3$–0.4, corresponding to high alignments of the order of 50–80% and more. The orientation mechanism in fusion–evaporation is well understood [138] and can be described in a classical way by the transfer of longitudinal projectile momentum to angular momentum in the compound nucleus. If the reaction products are selected at an angle with respect to the incoming projectile beam, a spin-polarized ensemble can be obtained, reaching polarizations up to 40% [139].

- In transfer reactions combined with IF mass separation, high amounts of spin-orientation have been established (∼30–40% [140]) but very rarely such reactions have been used to study moments of exotic nuclei. That is because the production yield of exotic nuclei is obviously higher in the intermediate- and high-energy projectile-fragmentation reactions. However, the much higher orientation obtained in these lower energy transfer reactions should not be forgotten, as the figure of merit for a nuclear moment measurement goes with the amount of orientation squared.
- Fragments produced in an intermediate- or high-energy projectile-fragmentation reaction are spin-aligned (if selected in the forward direction with respect to primary beam) [141–143] or spin-polarized (if selected at a finite angle with respect to the primary beam direction) [144–146, 133]. Typical values here are of the order of 10–20% of spin-orientation. However, the mechanism is still not fully understood and it is not yet possible to make predictions on the optimal conditions and the amount of orientation that can be obtained.
- Recently, the orientation of spontaneous fission fragments has been investigated [147] and applied in the measurement of isomeric g factors for very short-lived states using a time integral perturbed angular distribution measurement [148]. A prolate spin-orientation is found with the symmetry-axis along the fission axis.

5. Methods to study moments of radioactive nuclei: present status and future perspectives

A review of some currently available methods to study nuclear moments is given, and special attention is paid to recently developed techniques or to well-established methods which were adapted to the new production methods, to new spin-orientation methods or to the highly efficient detection systems that became available the last decades, such that now the study of static moments of very exotic nuclei has become possible. Each technique is applicable to particular types of nuclear states or elements and, at the end of this section, the regions of applicability are compared for a few methods.

5.1. General introduction and the angular distribution of radiation

The interaction of the nuclear magnetic dipole moment with a magnetic field and the interaction of the electric quadrupole moment with an electric field gradient are the basic ingredients of all methods to study nuclear moments. Nuclear moment measurements require, therefore, a strong interplay between nuclear physics, atomic physics, solid state physics and laser physics. The applied techniques are all based on a combined expertise in some of these fields, as will be demonstrated in the following examples. Each element has its specific chemical properties, each nuclear state its specific lifetime, decay mode and spin, and these properties will define which method is suitable for the study of its nuclear magnetic and quadrupole moment.

At the atomic level, the magnetic dipole interaction and electric quadrupole interaction between the nuclear moments and the fields induced by the electrons will give rise to a hyperfine splitting of the electronic states in free (stable or radioactive) atoms (figure 12). By investigating

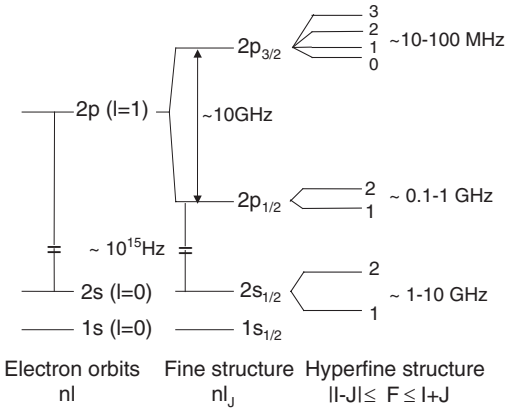

Figure 12. Electron levels are characterized by a fine structure (due to the l–s coupling of the orbital and spin electron angular momenta). The interaction of the electronic spin J with the nuclear spin I gives rise to hyperfine levels characterized by the total spin F in the atomic level scheme. The strength of the splitting is proportional to the nuclear magnetic moment. For a nuclear and electronic spin larger than $\frac{1}{2}$ the hyperfine splitting is also sensitive to the nuclear quadrupole moment.

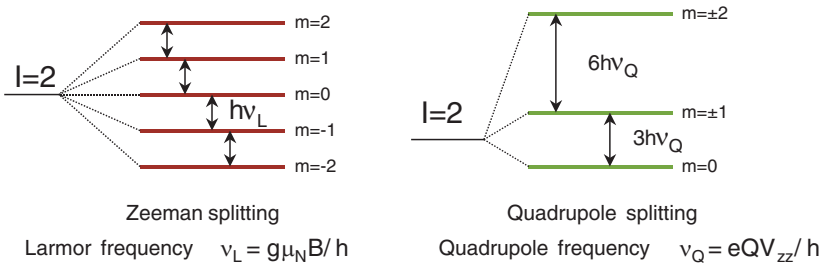

Figure 13. (*a*) Zeeman splitting of the nuclear m-quantum levels due to interaction of the nuclear dipole moment ($\mu = gI\mu_N$) with a static magnetic field B. In a classical picture this can be seen as a precession of the spin I around B with a Larmor frequency ν_L. (*b*) Non-equidistant quadrupole splitting of the nuclear m-quantum levels due to interaction of the nuclear spectroscopic quadrupole moment Q_s with an EFG V_{zz}.

this electronic hyperfine splitting, one can deduce the nuclear dipole and quadrupole moment, the nuclear spin and the change in mean square charge radius between two isotopes of the same element. Such measurements are done using many different laser techniques, adapted to the production method of the nuclei, the chemical properties of the element, etc [149–154]. Several detection methods can be distinguished for the measurement of the atomic hyperfine structure: optical detection (from decay of an electronic level), radioactive detection (from decay of a nuclear level), particle-detection (of resonantly ionized atoms).

At the nuclear level, the interaction between the nuclear spin (and moments) and the applied electromagnetic fields will induce a breakdown of the degeneracy of the nuclear m-quantum states. The Zeeman splitting (figure 13(*a*)) is induced by applying a static magnetic field, while the quadrupole splitting (figure 13(*b*)) is induced by implantation of the nuclei in a crystal with an electric field gradient (EFG). A typical energy splitting of nuclear quantum levels is of the order of nanoelectronvolts (corresponding to a MHz frequency range). To investigate such a small nuclear level splitting, which is again sensitive to the nuclear moments

and spin, different experimental techniques have been developed. For radioactive nuclei these techniques are based on the detection of an anisotropic distribution of the radioactive decay (γ, β, α), which requires that the ensemble of nuclear spins has a preferred orientation in space. Therefore, methods to orient the ensemble of radioactive nuclei are of crucial importance for such studies. The orientation techniques are closely related to the production and selection mechanisms for radioactive nuclei, as was illustrated in previous section.

In experiments based on the detection of the β or γ decay of a radioactive nuclear state, the angular distribution of the emitted radiation is the basic ingredient. The direction in which the β or γ radiation is emitted, is related to the direction of the nuclear spin. The relation which expresses the angular distribution of radiation emitted in a particular direction (θ, φ) with respect to a chosen axis system is given by [74, 75, 123]:

$$W(\theta, \varphi, t) = \sum_{k,n} \frac{\sqrt{4\pi}}{\sqrt{2k+1}} U_k A_k(\gamma, \beta, \ldots) B_k^n(I, \omega_L, \omega_Q, t) Y_k^n(\theta, \varphi) \qquad (5.1)$$

A_k are the radiation parameters describing the type of radiation and its properties, B_k are the orientation tensors of order k: they describe the orientation of the ensemble spin, and its change due to interaction with the surrounding fields. It is this parameter that needs to be calculated to describe the influence of a particular interaction on the spin-orientation. We will give some expressions for perturbed orientation tensors in some particular experiments. Y_k are the spherical harmonics: they depend on the position of the detectors with respect to the chosen axis system (the same as in which the interaction with the fields is described). U_k are the de-orientation coefficients, which take into account the loss of orientation in the ensemble, due to preceding non-observed radiation from the nuclear level under investigation (e.g. an isomer decaying via a fast cascade, in which the anisotropy of the lowest level is investigated).

The angular distribution function can be simplified for particular types of radiation. If γ radiation is detected, only radiation parameters with k = even are non-zero and the angular distribution is reduced to even order tensor components. Consequently, only alignment $(B_2, B_4, \ldots)$ can be measured by γ radiation.

If the nucleus is decaying by β decay, one can generally reduce the angular distribution function to the first-order tensor (for allowed β decay only $A_1 \neq 0$), which means that β decay is mainly sensitive to nuclear polarization. Furthermore, if one puts the detectors at 0° and 180° with respect to the axial symmetry-axis of the system (chosen as the Z_{lab}-axis), then only $n = 0$ tensor components are non-zero and thus the angular distribution function for β decay simplifies to:

$$W(\theta, \varphi, t) = 1 + A_1 B_1(I, \omega_L, \omega_Q, t) \cos\theta \qquad (5.2)$$

The orientation tensor of a system perturbed by some interactions, can be described as a function of the perturbation factors $G_{kk'}$ and the initial orientation tensor $B_k(I, t = 0)$ as follows:

$$B_1^0(I, \omega_L, \omega_Q, t) = \sum_{k,n} G_{1k}^{0n}(I, \omega_L, \omega_Q, t) B_k^n(I, t = 0) \qquad (5.3)$$

This expression shows that in order to be able to measure an odd tensor orientation (polarization) one needs to have initial polarization, unless an interaction is applied which allows transforming alignment into polarization (thus $G_{12}^{0n}(I, \omega_L, \omega_Q, t) \neq 0$). We will see in the next paragraphs that this requires some special features of the applied interactions. The formalism that allows the perturbation factor to be calculated, will be explained by applying it for the most complicated case of combined interactions (the level mixing perturbation factors). For the other experiments a similar approach can be used to deduce an expression for the perturbed angular

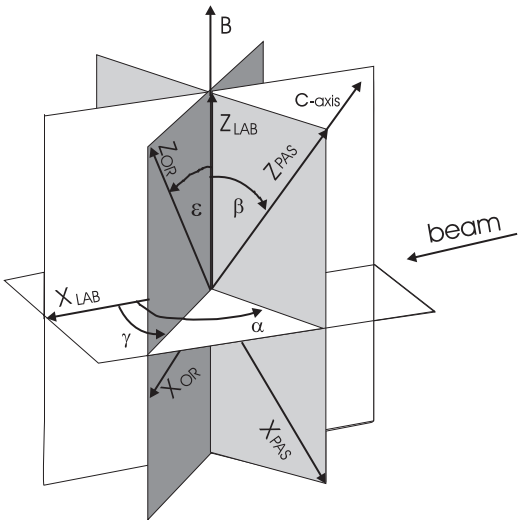

Figure 14. Definition of reference systems related to the perturbed angular distribution of oriented nuclei. The positions of the detectors are defined in the LAB. The initial spin-orientation is expressed in an OR-axis system with the Z_{OR} axis along the axial symmetry-axis of the orientation. It is most convenient to describe the electric quadrupole interaction with respect to the PAS of the EFG, which does not necessarily collide with the LAB system.

distribution. In these calculations, it is most convenient to express the initial (unperturbed) orientation of the ensemble in a reference frame that reflects the symmetry of the oriented ensemble (we will call this the OR-axis system). The Hamiltonian of the perturbing interactions is best described in a reference frame based on the symmetry in these interactions. If possible, this reference frame can be chosen to coincide with the laboratory axis (LAB) system that determines the positions of the detectors. In the angular distribution all tensors need to be transformed into the same axis system, by applying Euler rotations. An example of the reference frames relevant for a combined interaction experiment is given in figure 14.

5.2. Moments of exotic ground states from projectile fragmentation

The discovery of the presence of spin-polarization [144] and spin-alignment [141] in a selected ensemble of secondary projectile fragments was a major breakthrough in the study of nuclear moments of very exotic nuclei far from stability, in particular for neutron-rich nuclei. Using the spin-orientation obtained during the reaction process, nuclear moments of very short-lived states (down to the TOF in the mass separator, typically 200 ns) can be studied. Although the spin-orientation process is not yet fully understood, several groups have started to use this orientation to measure changes in the β decay asymmetry of exotic nuclei and the γ decay anisotropy of isomeric states, from which then information on the nuclear g factor and spectroscopic quadrupole moment can be extracted. While most groups have focused on using spin-polarized beams, our group has developed some techniques that allow taking advantage of the full yield of forward emitted fragments that are purely spin-aligned. In this contribution, we give an overview of the techniques that are being applied at several fragmentation facilities to study the moments of β decaying ground states produced in projectile fragmentation. We describe the basic interactions involved in each technique and how one can deduce the nuclear moments from the obtained experimental data. A general description on the experimental

set-up and data taking are given. Different variants of a technique have been developed on sometimes a case-by-case basis in order to optimize the signal-to-noise ratio, the efficiency of data taking, the efficiency of polarization destruction and detection, etc. We will not give details on each of these 'variants' on a technique, but give to the reader some references where further details can be found.

5.2.1. Rotation of the nuclear spins during recoil separation. For nuclei oriented in a nuclear reaction we can distinguish two situations to describe the spin-orientation immediately after the target, depending on the symmetry of the selected recoil beam with respect to the primary beam [155]. When the recoiling nuclei are selected symmetrically around the projectile beam direction, then due to symmetry considerations the ensemble of recoils will have their spins oriented around the beam axis, which is thus an axis of symmetry for an aligned ensemble of recoils (Z_{ORA}). In case the recoiling nuclei are selected under an angle with respect to the projectile beam direction, then the ensemble of recoils is spin-polarized with the polarization axis perpendicular to the reaction plane (plane of the incoming projectile beam and selected recoil beam). In that case, the orientation symmetry-axis (Z_{ORP}) is perpendicular to the beam direction. This is illustrated in figure 15 where we consider a primary beam that is deflected in the vertical direction, in order to select a polarized ensemble of fragments at a finite angle with respect to the beam direction. In most real situations the deflection occurs in the horizontal plane, thus inducing a polarization symmetry-axis in the vertical direction.

After the target, the recoiling fragments (or fusion–evaporation residues) are separated from the other reaction products by some electric or magnetic fields. In the dipole magnets the spins of the nuclei (assuming fully stripped nuclei) will precess with the Larmor frequency $\omega_{\mathrm{L}} = -g\mu_{\mathrm{N}}B/\hbar$, while the positively charged ions rotate with a frequency $\omega_{\mathrm{C}} = qB/m$ (the cyclotron frequency induced by the Lorenz force). After the recoil separation process the beam has rotated over an angle θ_{C} (determined by the rotation angles of all dipole magnets between the target position and the implantation position). The spin will have rotated over an angle $\theta_{\mathrm{L}} = \omega_{\mathrm{L}}t = \theta_{\mathrm{C}}\omega_{\mathrm{L}}/\omega_{\mathrm{C}}$. The alignment symmetry-axis will thus make an angle γ_{A} with respect

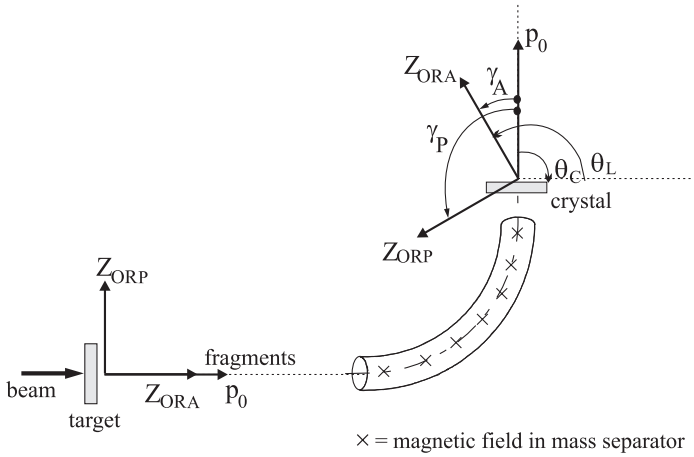

Figure 15. After recoil separation the symmetry-axis of orientation does no longer coincide with the beam axis. The Euler angles to transform the LAB to the orientation axis system (OR) are, respectively (ε_{A}, γ_{A}, 0) for aligned fragments and (ε_{P}, γ_{P}, 0) for polarized fragments.

to the beam axis:

$$\gamma_{\mathrm{A}} = \theta_{\mathrm{C}} + \theta_{\mathrm{L}} = \theta_{\mathrm{C}} \left(1 - \frac{gA}{2q}\right) \tag{5.4}$$

and the polarization axis will in this particular case make an angle γ_{P}:

$$\gamma_{\mathrm{P}} = \pm 90^{\circ} + \theta_{\mathrm{C}} \left(1 - \frac{gA}{2q}\right) \tag{5.5}$$

Notice that the deviation of the orientation axis is determined by the nuclear g factor, by the nuclear mass A and by the charge q of the selected ions (preferably fully stripped fragments, $q = Z$, to avoid loss of orientation via the hyperfine interaction during the flight in vacuum).

As we observe the orientation of the nuclei in the LAB system, a transformation of the orientation tensors from the OR frame to the LAB frame needs to be performed. In the OR frame the ensemble orientation has only $n = 0$ components (due to the axial symmetry) and the transformation to the LAB system can thus be reduced to following expression [27]:

$$B_k^n(I, t = 0)_{\mathrm{LAB}} = \sqrt{\frac{4\pi}{2k+1}} \mathrm{e}^{\mathrm{i}n\gamma} Y_k^n(\varepsilon, 0) B_k^0(I, t = 0)_{\mathrm{OR}} \tag{5.6}$$

5.2.2. β-NMR measurements on spin polarized fragment beams. In a β-NMR measurement on exotic projectile fragments, a pure beam of an exotic radioactive isotope is selected by the fragment separator (the typical beam purity varies between 70% and 99%). This beam is implanted in a stopper material, which is immersed into a static magnetic field. The Hamiltonian for the magnetic dipole interaction is $H_{\mathrm{B}} = -\boldsymbol{\mu}\boldsymbol{B_0} = -h\nu_{\mathrm{L}}\boldsymbol{I}_z$ if the Z-axis is chosen along the static magnetic field direction. The energy of the m-quantum states is then linear in m: $E_m = -h\nu_{\mathrm{L}}m$ and proportional to the Larmor frequency (figure 13). In NMR experiments, the static magnetic field is applied along the axial symmetry-axis of the spin-oriented ensemble. It is important to maintain this spin-orientation after implantation in the host crystal for at least one nuclear lifetime, or at least not to lose this orientation by interactions with 'uncontrolled' electromagnetic fields. Two types of such orientation-destroying interactions that often occur after implantation, are the spin–lattice relaxation interaction and interactions with defect-associated EFGs. Different types of relaxation mechanisms occur in different materials [156, 157]. For example, in metals the relaxation is mainly due to spin–spin interactions with the conduction electrons and the relaxation time increases with decreasing temperature (the Korringa relation [158]). To maintain the spin-orientation after implantation it is important to choose a host material in which the spin-lattice relaxation time is longer than the nuclear lifetime. Spin-lattice relaxation times can vary from 10^{-4} to tens of seconds. For long-lived isotopes implanted in a metal, it might be useful to cool down the implantation host to liquid He-temperature, in order to enhance the relaxation time by two orders of magnitude.

The host material needs to have a cubic lattice structure, in order not to induce an EFG on the position of the implanted isotopes (see next paragraph). Care must be taken that the element of interest implants well in the chosen crystal, such that no defect-associated EFGs are induced by, e.g. vacancies in the region of the implanted nucleus. The chemical properties of both the impurity and the host elements play a role in this, such as the electro-negativity and the radii of the involved atoms [159]. By applying a strong enough static magnetic field along the spin-orientation symmetry-axis, the interaction with small defect-associated EFGs can be neglected in some cases (typical fields of order of a few 100 Gauss are needed). Strong defect-associated EFGs cannot be neglected, and can even be used as an advantage in some particular type of experiments [160].

If all isotopes are submitted to the same homogeneous magnetic field B_0 they all precess with the same Larmor frequency and they all exhibit the same Zeeman splitting of the nuclear

m-quantum levels (figure 13). The different quantum states are unequally populated due to the spin-orientation of the selected ensemble. In an NMR experiment, the implanted radioactive nuclei are submitted additionally to a radio-frequency (RF) magnetic field, which is applied perpendicular to the static magnetic field. By adding a RF field $B_1(t)$ in the plane perpendicular to the static field, the Hamiltonian is no longer axially symmetric and thus the $|m\rangle$ states are no longer eigenstates of H. It can be shown [161] that this breaking of the axial symmetry will cause a mixing of the $|m\rangle$ state populations if the RF matches the Larmor frequency. At that moment, the level populations p_m are all equalized. This resonant destruction of the spin-orientation, which occurs when the applied RF ν_{RF} matches the Larmor frequency ν_{L} of the nuclear spins (figures 13(a) and 16), can be visualized via the β decay. Due to the parity violation of the β decay, a polarized ensemble of radioactive nuclei will emit electrons (or positrons) in a preferential direction with respect to the spin direction [123]. Consequently, a polarized ensemble will give rise to an asymmetric angular distribution. By detecting the resonant destruction of the polarization in the β-asymmetry, one can thus get information on the nuclear g factor. Such a measurement can be performed as a function of the static magnetic field strength B_0 (keeping the RF constant) or as a function of the applied RF (keeping the static field constant, figure 16). Note that for a low RF field strength only $\Delta m = 1$, one-photon transitions, can be induced. However, for RF field strengths of several Gauss one should also be aware of two-photon transitions between $\Delta m = 2$ states, giving rise to resonances at twice the Larmor frequency.

Different types of NMR experiments can be distinguished, as discussed in several recent experiments, using pulsed or continuous implantation of projectile fragments, using a frequency-modulated or non-modulated RF field, etc [145, 162, 163]. In a β-NMR experiment, it is important that the ensemble is spin-polarized, because the destruction of spin polarization is the signature from which the nuclear g factor is deduced. Because a polarized ensemble requires selection of fragments at a finite angle with respect to the primary beam direction, the intensity of the polarized fragment beam is reduced by a factor of ∼5 as compared to the

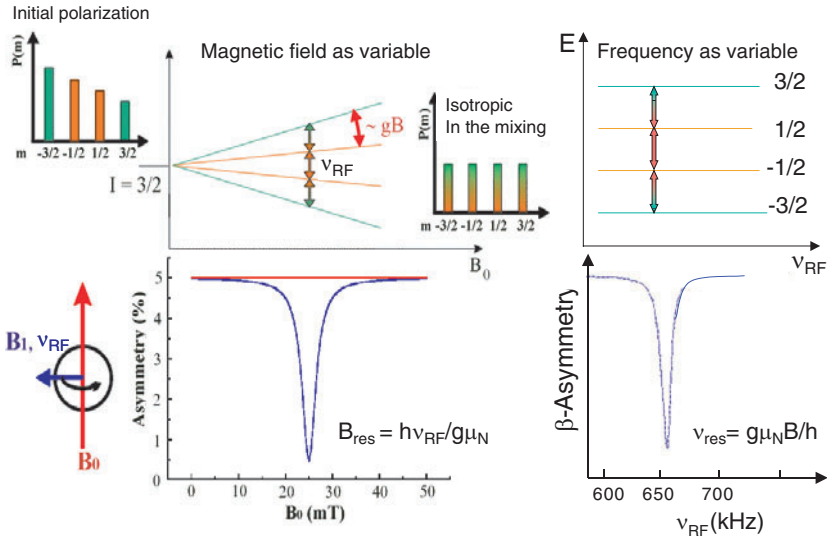

Figure 16. The nuclear g factor can be deduced from a measurement of the resonant destruction of the asymmetry in the β decay of a polarized ensemble submitted to a static and RF magnetic field.

intensity of a forward selected (aligned) secondary beam. A method that allows using a spin-aligned fragment beam to investigate NMRs in the β decay is suggested in [164], by applying an additional EFG, next to the static and RF magnetic fields. It can be shown that by combining these interactions, spin-alignment is resonantly transferred into spin-polarization and this can be observed as a resonant onset of asymmetry in the β decay [155]. Details on the level mixing resonance (LMR) method, which is the basis for this new β-NMR-LMR method, are given in section 5.2.4. Although the β-NMR-LMR method takes advantage of the full intensity of the forward selected beam, the amount of resonantly induced spin-polarization (determining the amplitude of the measured signal) is less than the amount of resonantly destroyed polarization in a standard NMR experiment. The intensity gain is not always enough to compensate for this loss, except for nuclei with spin $I = 1$ as illustrated in [165].

5.2.3. β-nuclear quadrupole resonance measurements on spin polarized fragment beams. The same type of experiment can be performed, with the difference that the selected fragment beam is stopped in a material with a non-cubic lattice structure. In a non-cubic crystal lattice an EFG is induced at the position of the implanted nuclei. This field gradient will interact with the non-spherical charge distribution of the implanted nucleus (reflected by a non-zero spectroscopic quadrupole moment Q_s). The Hamiltonian of the quadrupole interaction is conveniently described in a reference frame fixed to the principle axis system (PAS) of the EFG, characterized in this case by a strength V_{zz} and an asymmetry parameter η [166]. If the EFG is axially symmetric ($\eta = 0$) the interaction Hamiltonian is described by

$$H_Q = \frac{\omega_Q}{\hbar}(3I_z^2 - I^2), \qquad \text{with } \omega_Q = \frac{eQVzz}{4I(2I-1)\hbar} \tag{5.7}$$

the quadrupole interaction frequency, which is related to the quadrupole coupling constant ν_Q:

$$\nu_Q = \frac{eQVzz}{h} = \frac{\omega_Q 4I(2I_1)}{2\pi} \tag{5.8}$$

The projection of the spin-operator onto the Z-axis of the PAS is an eigenstate $|m\rangle$ of this Hamiltonian with eigenvalue $E_m = \hbar\omega_Q[3m^2 - I(I+1)]$, represented in figure 13(b). The $|-m\rangle$ and $|+m\rangle$ levels are degenerate in this case. An RF-field $B_1(t)$ applied in the plane perpendicular to the symmetry-axis of the EFG will again cause a mixing of the $|m\rangle$ states, in this case if the RF $\omega_{RF} = 2\pi\nu_{RF}$ matches one of the quadrupole splitting frequencies (for single photon transitions):

$$\Delta\omega_Q = 3(2m-1)\omega_Q = \omega_{RF} \tag{5.9}$$

At that moment, the level populations of two levels p_m and p_{m+1} are equalized and this change of the spin-orientation can be detected in the asymmetry of the radioactive decay. However, if the populations of the $|m\rangle$ and $|m+1\rangle$ levels are equalized by the RF, the p_{-m} and p_{-m-1} are also equalized because the $\pm m$ levels are degenerate in case of a pure quadrupole interaction. Thus, a change in the polarization ($p_m \neq p_{-m}$) can only be detected if the spins are polarized before the RF-interaction takes place. A destruction of the initial polarization can then be induced by the RF-interaction which will mix the population of levels with $\Delta m = 1$. By looking for the resonance frequencies ν_{RF} at which the spin-orientation is modified, one can thus determine the quadrupole interaction frequency using relation (5.9) (see also figure 13(b)). If the EFG can be determined by some other technique, the nuclear quadrupole moment Q_s is deduced. The experimental technique in which the asymmetry of the β decay is changed due to a quadrupole interaction, and in which this change is measured as a function of the applied RF is called the nuclear quadrupole resonance (NQR) method. In most NQR-experiments an additional external magnetic field is applied along the EFG symmetry-axis, in order to preserve

the spin-polarization more easily after implantation. The Hamiltonian for such a combined collinear interaction is discussed in section 5.2.4 and the similarities and differences between NQR and LMRs observed for non-collinear interactions are extensively discussed in [164]. When a combined interaction is applied, NQRs are observed in the measured β-asymmetry as a function of the applied RF, each time the RF matches the frequency separation of two quantum levels:

$$\omega_{\mathrm{RF}} = 3\omega_Q(2m-1) + \omega_{\mathrm{L}} \tag{5.10}$$

Because in this case the populations of only two m-quantum states (E_m and E_{m-1}) are mixed by the applied RF-interaction, the method can be applied to spin-aligned projectile fragments as well, as discussed in [164]. Over the years, several highly sophisticated versions of the NQR technique have been developed in order to enhance the detected change in β decay asymmetry. An example is the method of multiple frequency NQR [167, 168].

5.2.4. β-LMR measurements on projectile fragments. When the selected fragment beam is implanted in a crystal with an EFG and at the same time the crystal is immersed in a static magnetic field, the nuclear spins will be interacting with both fields and thus be submitted to a combined interaction. The Hamiltonian of such a combined interaction can be expressed in an axis system fixed to the static magnetic field (the LAB system) [169] or with respect to the PAS system of the EFG [170]. The former is appropriate when making a full numerical calculation of the eigenstates of this Hamiltonian, as they are immediately expressed in the LAB reference frame. However, more insight into the properties of a combined interaction are obtained by expressing the Hamiltonian in the PAS frame. By decoupling the magnetic interaction into components along and perpendicular to the Z_{PAS}-axis, and for an axially symmetric EFG we get:

$$\begin{aligned} H &= H_{\parallel} + H_{\perp} \\ &= \frac{\omega_Q}{\hbar}(3I_{\mathrm{Zpas}}^2 - I^2) + \omega_{\mathrm{L}}\cos\beta I_{\mathrm{Zpas}} - \omega_{\mathrm{L}}\sin\beta I_{\mathrm{Xpas}} \end{aligned} \tag{5.11}$$

If the crystal is oriented such that the EFG collides with the direction of the magnetic field ($\beta = 0$), the Hamiltonian is axially symmetric around the Z_{PAS} axis. Then the eigenstates of the spin-operator $\boldsymbol{I}_{\mathrm{Zpas}}$ are also eigenstates of the Hamiltonian and the energy of these $|m\rangle$ states is:

$$E_m = \hbar\omega_Q(3m^2 - I(I+1)) + \hbar\omega_{\mathrm{L}}m \tag{5.12}$$

These energy levels can be calculated as a function of the static magnetic field strength, as represented in figure 17(a) for a nucleus with spin $I = \frac{3}{2}$. At particular values of the magnetic field we see that two quantum states are crossing (thus having degenerate energy levels). This crossing of energy levels E_m and $E_{m'}$ occurs at equidistant values of the magnetic field strength B, namely if:

$$\omega_{\mathrm{L}} = 3(m+m')\omega_Q \quad \Rightarrow \quad \frac{\nu_{\mathrm{L}}}{\nu_Q} = \frac{3(m+m')}{4I(2I-1)} \tag{5.13}$$

The spin of the nucleus determines the number of eigenstates $|m\rangle$ and thus the number of level crossing points. Furthermore, the distance between two crossing fields depends on the spin and is the same between all crossing fields:

$$\frac{3}{4I(2I-1)} \tag{5.14}$$

When the crystal EFG is not placed parallel to the magnetic field ($\beta \neq 0$), then the $|m\rangle$ quantum states are no longer eigenstates of the Hamiltonian because the axial symmetry has been broken.

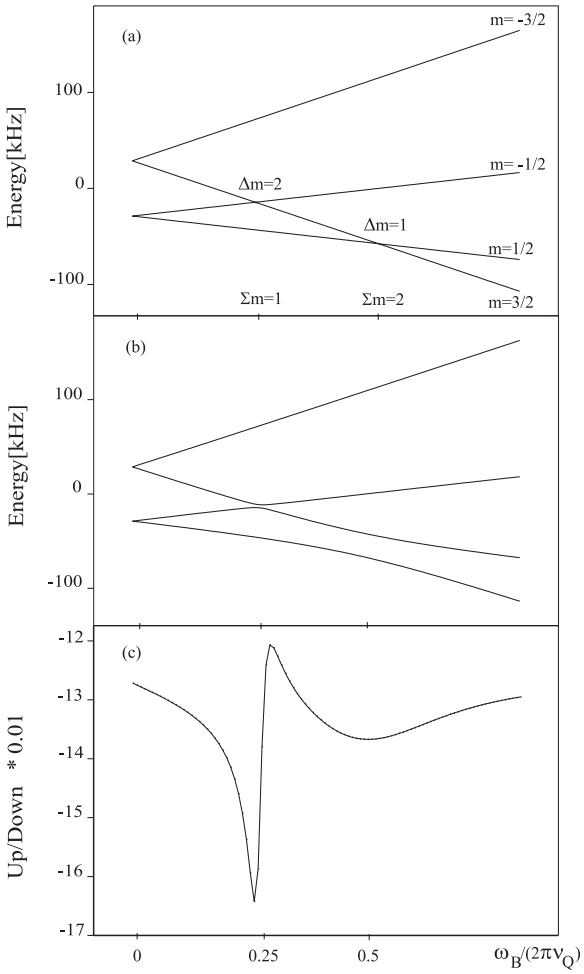

Figure 17. (*a*) A Breit–Rabi diagram of a nucleus with spin $I = \frac{3}{2}$ and tilt angle $\beta = 0^\circ$, (*b*) similar for a tilt angle $\beta = 15^\circ$. When the populations of the hyperfine levels mix, the levels repel each other. (*c*) The up/down asymmetry in the nuclear β decay as a function of a static magnetic field for $\beta = 15^\circ$, $B_1 = 0.2$, $B_2 = 0.2$, $\gamma_A = 2^\circ$, $\varepsilon_P = 90^\circ$ and $\gamma_P = 92^\circ$.

When the tilt angle β is small ($<20^\circ$), the last term in the Hamiltonian (5.11) can be considered as a small perturbation on the unperturbed energy levels (5.12). The eigenstates and energy of the total Hamiltonian can be derived in first-order quasi-degenerate perturbation theory [171] in a 'two-level' approximation [170, 172, 104]. This means that, in a first approximation, we can assume that the energy of the perturbed states is similar to the energy of the unperturbed states except for two nearly-degenerate energy levels. The energy near two crossing levels $|m\rangle$ and $|m'\rangle$, with $|m - m'| = \Delta m$, will be significantly perturbed and the perturbed eigenstates are:

$$\begin{aligned} |N\rangle &= \frac{1}{\sqrt{1+R^2}}(|m\rangle - R|m'\rangle) \\ |N'\rangle &= \frac{1}{\sqrt{1+R^2}}(R|m\rangle + |m'\rangle) \end{aligned} \tag{5.15}$$

We call them 'mixed' eigenstates because they consist of a mixing of the two unperturbed levels. Their energies are repelling each other:

$$E_{N,N'} = \frac{E_m + E_{m'}}{2} \pm \frac{1}{2}\sqrt{(E_m - E_{m'})^2 + 4(W_{mm'}^{\Delta m})^2} \tag{5.16}$$

The mixing parameter R depends on the non-diagonal matrix element [172] which induces an interaction between the $|m\rangle$ and $|m'\rangle$ levels. This perturbation is proportional to:

$$W_{mm'}^{\Delta m} \sim \langle m|(H_\perp)^{\Delta m}|m'\rangle \sim (\sin\beta)^{\Delta m} \tag{5.17}$$

At the level mixing field, determined by $\omega_L = 3(m + m')\omega_Q \cos\beta$, the mixing parameter is $R = 1$ and the two levels are fully mixed [172]. One can calculate in a density matrix formalism that the level populations have become equal, as demonstrated further in equation (5.23). In figure 18, the unperturbed levels $E_{m,m'}$ and the mixed levels $E_{N,N'}$ are shown near a level crossing, as a function of the magnetic field strength. Note that the amount of repelling (anti-crossing) between the mixed levels depends on the perturbation strength $H_\perp$ and thus on $(\sin\beta)^{\Delta m}$. This will also determine the width (Γ) of the mixing region as a function of the field, and thus the width of the related LMR in the angular distribution (see later). This means that we can choose ourselves the mixing strength (and thus the resonance width) by placing a particular angle β between the c-axis of the crystal and the magnetic field direction. In figure 17(b) the energy levels of the level mixing Hamiltonian (5.11) have been calculated by a numerical diagonalization procedure over a wide range of magnetic fields, covering all mixing regions.

To calculate the perturbation of the ensemble orientation one has to solve the time evolution equation of the nuclear density matrix:

$$i\hbar\frac{\partial\rho}{\partial t} = [H, \rho] \tag{5.18}$$

with H the level mixing Hamiltonian (5.11). To solve this equation, one needs to find first the eigenstates $|N\rangle$ and eigenvalues E_N of the interaction Hamiltonian. If the Hamiltonian is expressed in the LAB frame the eigenstates are found by numerical diagonalization. In that case one gets the eigenstates $\langle N \mid m\rangle$ with respect to the LAB system and they can be introduced in the perturbation factors to calculate numerically the angular distribution function (see next paragraph).

In this section, we will use the analytical expression (5.15) of the mixed eigenstates with the Hamiltonian expressed in the PAS, to demonstrate how the perturbing interaction influences the level populations (and thus the ensemble orientation). This will allow us to get

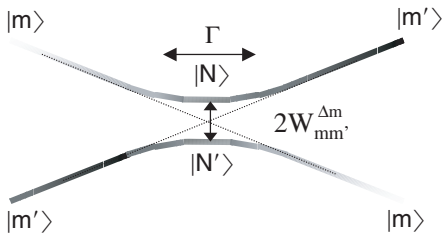

Figure 18. In a two-level approximation the eigenstates of the level mixing Hamiltonian can be calculated using perturbation theory. Near the crossing region of the unperturbed levels (E_m eigenvalues of $H_\parallel$) the symmetry breaking part of the interaction ($H_\perp$) is mixing the states: the eigenstates of H are linear combinations of the unperturbed states. The respective energies are repelling each other near the crossing region.

an explicit expression for the time-dependence of the density matrix and thus to understand better the nature of the resonances that will appear in the angular distribution of the β decay. For a static interaction, such as the level mixing interaction, the solution of the Von Neumann equation (5.18) is given by

$$\langle N|\rho(t)|N'\rangle = \rho_{NN'}(t) = \mathrm{e}^{-\mathrm{i}\omega_{NN'}t}\rho_{NN'}(0) \tag{5.19}$$

with $\omega_{NN'} = (E_{\mathrm{N}} - E_{N'})/\hbar$ and $E_{N,N'}$ given by (5.15). As the LMR method is a time-integrated measuring technique, we need to calculate the time-averaged density matrix taking into account the nuclear decay time:

$$\rho_{NN'}(\tau) = \frac{\int_0^\infty \mathrm{d}t\ \rho_{NN'}(t)\mathrm{e}^{-t/\tau}}{\int_0^\infty \mathrm{d}t\ \mathrm{e}^{-t/\tau}} = \rho_{NN'}(0)\frac{1 - \mathrm{i}\omega_{NN'}\tau}{1 + (\omega_{NN'}\tau)^2} \tag{5.20}$$

It is more convenient to express the density matrix in the m-representation. Using the orthogonality relation, the time-integrated density matrix in the m-representation is:

$$\begin{aligned}\rho_{mm'}(\tau) &= \sum_{NN'} \langle m \mid N\rangle \rho_{NN'}(\tau)\langle N' \mid m'\rangle \\ &= \sum_{NN'} \langle m \mid N\rangle\langle N' \mid m'\rangle \frac{1 - \mathrm{i}\omega_{NN'}\tau}{1 + (\omega_{NN'}\tau)^2}\rho_{NN'}(0)\end{aligned} \tag{5.21}$$

The density matrix of the initial orientation tensor $\rho(0)$ is not known in the $|N\rangle$-basis. It is best described with respect to a reference frame in which the symmetry of the ensemble orientation is reflected, as described in section (4.1.1). This density tensor is then easily transformed into a density tensor expressed in the PAS, using the rotation properties of the orientation tensor (5.6). From this rotated density tensor, the density matrix $\rho_{mm'}$ can be calculated using relation (4.1). The time-integrated perturbed density matrix is finally obtained from:

$$\rho_{mm'}(\tau) = \sum_{NN'} \langle m \mid N\rangle\langle N' \mid m'\rangle \frac{1 - \mathrm{i}\omega_{NN'}\tau}{1 + (\omega_{NN'}\tau)^2} \sum_{\mu\mu'} \langle N \mid \mu\rangle\langle \mu' \mid N'\rangle \rho_{\mu\mu'}(0) \tag{5.22}$$

Using the explicit expression for the eigenstates (5.15), eigenvalues (5.16) and R [172], we can calculate the time-averaged components of the density matrix of nuclei submitted to the level mixing interaction. The diagonal matrix elements are:

$$\rho_{mm}(\tau) = \rho_{mm}(0) + \tfrac{1}{2}\{\rho_{m'm'}(0) - \rho_{mm}(0)\}L_{mm'}(\tau) \tag{5.23}$$

and a similar expression is found for $\rho_{m'm'}(\tau)$ (by exchanging m and m'). $L_{mm'}$ is a Lorentz absorption resonance as a function of the unperturbed energy splitting:

$$L_{mm'} = \frac{(2W_{mm'})^2}{(E_m - E_{m'})^2 + (2W_{mm'})^2 + (\hbar/\tau)^2} \tag{5.24}$$

The time-averaged perturbed population probability $\rho_{mm}(\tau)$ given by expression (5.23) depends on the initial level population difference between the two mixing levels m and m'. For nuclei with a long enough lifetime τ the Lorentz function is 0 far from the crossing region, and becomes 1 in the centre (when $E_m = E_{m'}$). So if the level mixing condition $2W_{mm'} \gg \hbar/\tau$ is fulfilled, the amplitude of the LMR is independent of the nuclear lifetime and reaches a maximum (figure 19).

In Scheveneels *et al* [172] a detailed description of several features of this LMRs is given. For example, it is shown that the non-diagonal matrix elements of the density matrix show a resonant dispersive character. Each of these resonances can be detected in the angular distribution, if the proper configuration is chosen.

To introduce the orientation described by this perturbed density matrix into the angular distribution, we need to use the relation between the density matrix and the density tensor (4.1).

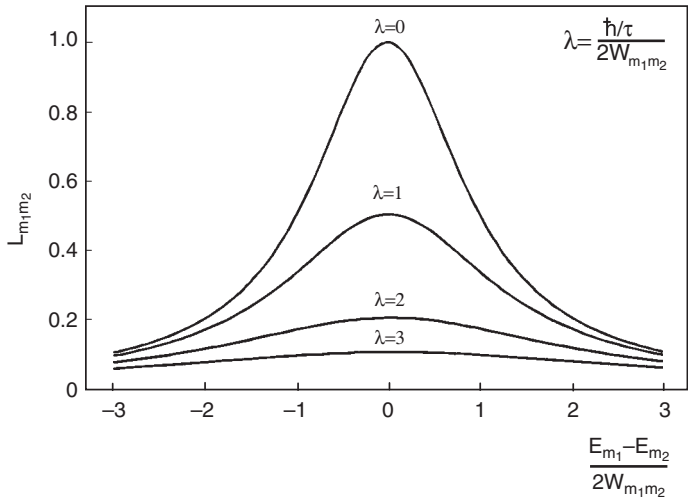

Figure 19. Simulation of the Lorentz absorption resonance as a function of the energy splitting near two crossing m-quantum states, for nuclei with different lifetimes. The full amplitude of the resonance curve is obtained only if the lifetime is significantly longer than the inverse perturbation strength.

We also need to specify the initial orientation more explicitly. As an example we will consider nuclei that are produced in a fragmentation reaction and selected in the forward direction with respect to the primary beam. An ensemble of spin-aligned projectile fragments is obtained, which in a first approximation we describe by one parameter $B_2^0 \sim A$ (4.4) in a reference frame with the Z-axis parallel to the axial symmetry-axis of the alignment (Z_{OR} in figure 15). After the fragment separation process, the OR-axis system is defined by some Euler angles $(\varepsilon, \gamma, 0)$ with respect to the LAB system (figures 14 and 15). For projectile fragments behind a doubly-achromatic dipole spectrometer (like LISE at GANIL), the alignment axis is lying in the (X, Y)-plane and thus $\varepsilon = 90^\circ$. The orientation tensor at the time and place of implantation $(t = 0)$ is then described by expression (5.4). In section 5.1.1, we have already shown how the angular distribution is related to the perturbed orientation tensors via the perturbation factors, using expressions (5.1)–(5.3). To derive an explicit expression for the perturbation factors, it is sufficient to transform expression (5.22) in its tensor form and to compare this with (5.3). The time-integrated G factors are given by:

$$G_{kk'}^{nn'}(\tau) = \hat{k}\hat{k}' \sum_{\substack{m,\,\mu \\ N,\,N'}} (-1)^{m-\mu} \begin{pmatrix} I & I & k \\ -m & m' & n \end{pmatrix} \begin{pmatrix} I & I & k' \\ -\mu & \mu' & n' \end{pmatrix}$$

$$\times \langle m \mid N\rangle\langle N' \mid m'\rangle\langle \mu \mid N\rangle^*\langle N' \mid \mu\rangle^* \frac{1 - \mathrm{i}\omega_{NN'}\tau}{1 + (\omega_{NN'}\tau)^2} \tag{5.25}$$

If the Hamiltonian is described in the LAB system, the perturbation factor is calculated in the LAB frame by determining the eigenstates and eigenfunctions of H numerically. In that case, the perturbed orientation tensor in (5.3) is also obtained in the LAB frame and the initial orientation tensor needs to be calculated also in this axis system. Introduction of all these functions into the angular distribution function allows numerical calculations of the decay anisotropy as a function of the magnetic field strength. An example of a full numerical calculation of the angular distribution for β decaying projectile fragments is given in figure 17(c).

In the future, this formalism could be extended to study the deformation of γ decaying isomeric states produced by projectile fragmentation. Such a formalism has already been developed and a proof of principle was performed for the case of isomers produced via fusion–evaporation reactions (see section 5.4.3). The technique has however not been further applied, because for isomers with a spin larger than about $5\hbar$ it is not possible to measure 'resonances' in the angular distribution, because too many of them occur (the amount of resonances is proportional to the spin). Therefore, a non-resonant variation on the γ-LMR method was developed. In the case of projectile fragmentation one could use both this non-resonant method to study high-spin isomers and the resonant γ-LMR for the study of low-spin ($I < 5\hbar$) isomers. Because the spin-orientation axis is not parallel to the beam axis, the existing formalism will have to be modified, and the optimal experimental set-up needs to be designed.

5.3. Moments of exotic nuclei from ISOL production schemes

5.3.1. Laser spectroscopy methods. Laser spectroscopy methods are very powerful tools to measure not only the static magnetic and quadrupole moment of exotic nuclei via their atomic hyperfine structure, but also to get information on the nuclear shape and radius from the isotope shift (relative to another isotope of the same element). Many variants of laser spectroscopy methods exist, and all these techniques are based on the interaction of a laser beam with the atomic electrons of exotic ions produced via different ISOL techniques. Information on the nuclear moments and shapes is deduced from scanning the frequency of the laser beam until resonant excitation of the atomic electrons is induced.

An overview of some former and recently developed laser spectroscopy methods can be found in [151, 153] as well as in the proceedings of a recent conference dedicated to this subject [173]. In this report, we focus on the most recent developments in the field, which are mainly related to laser spectroscopy on refractory elements.

A method was developed at ISOLDE/CERN [174] to study the hyperfine structure and isotope shifts of refractory elements not directly available as beams from the isotope separator, but as daughter products. By collecting a primary radioactive beam in some catcher, it is possible to produce a pure beam of refractory radioactive atoms by laser-desorption using resonant multiple-step laser ionization with a pulsed-laser beam. By delaying the laser-desorption as long as necessary, a particular daughter of interest can be obtained. Collaboration for spectroscopic measurements using a pulsed-laser ion source (COMPLIS) experiments have been carried out on very neutron-deficient gold, platinum and iridium isotopes. Magnetic moments, spectroscopic quadrupole moments, and changes of the nuclear mean square charge radii along each isotopic series have been extracted [175].

Recently, the method of collinear laser spectroscopy has been successfully applied for the first time on an ion-guide mass separator (IGISOL) at Yvaskyla, Finland [86]. With an ion guide, one can produce refractory elements (and short-lived nuclei) that cannot be obtained at the classical catcher–ionizer ISOL facilities. The main problem with the beams from an ion-guide ISOL facility is the large ion beam energy spread ($\sim$6 eV as compared to $\sim$1 eV for other ISOL facilities) which induces a large Doppler broadening in the collinear laser spectra. To increase the sensitivity of the laser spectroscopy technique a gas-filled linear Paul trap was installed on the beam line [176]. In this ion-trap a continuous low-energy ion beam is cooled and accumulated and subsequently released as a short (10–20 μs) bunch. This allowed improvement of the signal-to-noise ratio by a factor of 2×10^4 in collinear laser measurements, allowing spectroscopic measurements to be made with ion-beam fluxes of the order of 50 ions s^{-1}. With this method it was possible to study moments and radii of several isotopes of the refractory element Hf [154], as well as for a chain of $^{96-102}$Zr

isotopes produced by uranium fission and subsequently mass separated with the ion-guide method [177].

The third development in this field is related to the laser ion source at ISOLDE [178], in which for the first time resonance ionization spectroscopy has been performed [179, 180]. This in-source laser spectroscopy method allows the magnetic moments, spins and radii of exotic nuclei to be measured during the time of their production. This is an ideal method for studying moments of very rare isotopes (ground states or long-lived ms-isomers) in the heavier mass region (for low Z nuclei the hyperfine structure cannot be resolved due to the collisional broadening in the source).

5.3.2. Spin-oriented ISOL beams. If the ISOL beams can be polarized by some means, using the techniques suggested in section 4.2, then the methods to measure their moments are the same as the ones described in section 5.1 for the study of projectile-fragment moments. These methods are applicable to exotic nuclei with lifetimes between 10 and 10^4 ms. Examples of recent experiments on spin-oriented ISOL beams are the measurements of the nuclear moments of halo nuclei like ^{11}Li [121, 167] and ^{11}Be [122], as well as on neutron-rich Na isotopes [181] by using the optical pumping polarization method. With the tilted foils polarization method successful experiments were performed on ^{8}Li, ^{27}Si [182] and ^{23}Mg [132].

5.3.3. Moments of long-lived ISOL beams investigated via NMR-ON. A technique which has existed for many years, and which has been described in great detail in [123] is the low temperature nuclear orientation (LTNO) method to orient the spins of nuclei. Since the mid-eighties attempts have been made to combine this spin-orientation method with the on-line implantation of radioactive nuclear beams [183, 184], in order to perform moment measurements on exotic radioactive nuclei by looking at their anisotropic α, β or γ decay [185, 186]. The moments of exotic radioactive nuclei that have lifetimes of more than a second can be measured very precisely by applying the NMR or LMR methods [187] on these low-temperature oriented nuclei. However, as a temperature of the order of 100 mK is required in order to obtain the spin-orientation, it is not easy to combine this orientation method with on-line implantation, neither with the application of an RF-field for precision measurements (both induce some heat in the host crystal). This technique for measuring nuclear moments of ISOL produced beams is applicable to sufficiently long-lived exotic radioactive beams. It is complementary to the laser spectroscopy methods, as it allows precision measurements with an accuracy that can in most cases not be reached by laser spectroscopic techniques. Exotic nuclei which have recently been investigated by this method are situated around ^{132}Sn [187, 188] and around ^{68}Ni [189].

5.4. Moments of isomeric states with lifetimes between 1 ps and 1 ms

Several methods exist to study the magnetic and quadrupole moments of high-spin γ decaying isomeric states. Depending on the lifetime of the isomer, different techniques need to be applied.

To measure the magnetic moment of a nuclear excited state with a lifetime between 1 ps and 10 ns the transient field (TF) method [190–192] is a unique tool. For isomers with lifetimes between 10 ns and 100 μs the TDPAD method [193] is used to measure the g factor. For longer lived isomeric states (10 μs $< \tau <$ few milliseconds) a few experiments using the stroboscopic observation of nuclear Larmor precession [194] have been performed and for the longest lived isomers (>few ms), techniques as described for the ground state of exotic nuclei can be applied (although adapted to γ detection).

The static quadrupole moments of very short-lived excited states (<10 ns) have not been measured until now, because no suitable method exists. One usually relies on the measured lifetimes or B(E2) transition rates to determine the dynamical quadrupole moment and nuclear deformation of these states. A variation on the TDPAD method is used to study the static quadrupole moment of isomers with lifetimes in the nanosecond region. For the longer lived ($>10\,\mu$s up to a few milliseconds) high-spin isomeric states the recently developed LEMS method is more suitable [58] because it is not limited by the isomeric spin. This method can also be used for lifetimes down to 50 ns. Here, we briefly give the main aspects of some of these methods. In particular, we will discuss the LEMS method for long-lived high-spin isomers and the application of the TDPAD method to study moments of isomers produced in projectile fragmentation.

5.4.1. TDPAD method. The TDPAD method is probably one of the first methods, which has been used to study the magnetic moment of isomeric states. The method can also be used to study the quadrupole moment of these isomeric states, provided the isomers are produced (or recoiling) into a crystal with a non-cubic lattice structure (whereas they need to recoil into a cubic crystal structure to allow a g factor measurement). The method can be applied to isomeric states with lifetimes between 10 ns and about 100 μs. The lower lifetime limit is determined by the fact that the Larmor precession period needs to be smaller or of the order of the nuclear lifetime (thus requiring magnetic fields of the order of 1 T to allow a fast enough precession for short-lived isomers). It is also limited by the fact that the detection of γ radiation often requires the use of high-purity Ge detectors, which have a typical time resolution of only about 10 ns (in optimal conditions). The upper lifetime limit of the method is determined by spin–spin and spin–lattice relaxation effects, which induce a dephasing of the precession frequencies of the implanted nuclei and a time-dependent loss of spin-orientation.

In a TDPAD experiment a spin-oriented ensemble of isomeric states is implanted into a suitable (liquid or solid) host material with the appropriate lattice structure. In case of a g factor measurement, the host crystal is immersed in a sufficiently strong static magnetic field oriented perpendicular to the symmetry-axis of the ensemble orientation. The static field induces a Larmor precession of the nuclear spins. This spin precession gives rise to a time-dependent change in the angular distribution of the radiation emitted by the oriented isomeric states, which can be detected in a plane perpendicular to the magnetic field direction. The detection of γ radiation is sensitive to the even tensor components of the orientation tensor, so a change in alignment is detected. In a typical in-beam experiment, the time-dependent intensity of the emitted *gamma* radiation observed in a detector at an angle θ with respect to the alignment axis is given by

$$I(t, \theta, B) = I(t = 0)\mathrm{e}^{-t/\tau} W(t, \theta, B) \tag{5.26}$$

The perturbed angular distribution is in this case given by

$$W(t, \theta, B) = \sum_{k=\text{even}} U_k A_k(\gamma) B_k(I) P_k(\cos(\theta - \omega_{\mathrm{L}} t)) \tag{5.27}$$

with the different parameters as explained in section 5.1. In most of the cases, the product $A_k B_k$ is very small for $k < 4$ and, to a good approximation, the angular distribution is characterized by the coefficients A_2 and B_2 only. The argument of the cosine function reflects directly the fact that the nuclear ensemble has its orientation axis collinear to the beam axis.

The magnitude and the sign of the g factor can be extracted by measuring the intensity of emitted γ rays in detectors placed at 90° with respect to each other:

$$R(t,\theta,B) = \frac{I(t,\theta,B) - I(t,\theta+90,B)}{I(t,\theta,B) + I(t,\theta+90,B)} = \frac{3A_2B_2}{4+A_2B_2}\cos\{2(\theta-\omega_L t)\} \tag{5.28}$$

Note that the sign of the g factor cannot be extracted from the $R(t)$ function in the case of $\theta = 0°$, that means for a detector placed along the alignment axis. The in-beam TDPAD method requires a pulsed production of the isomeric states, thus using a pulsed primary beam with a period of $T_0 > \tau$ (the isomeric lifetime) and a pulse width ΔT much smaller than the Larmor period ($\Delta T_L = 1/\omega_L$). Due to the decreasing duty cycle ($\sim\Delta T/\tau$) for increasing isomeric lifetimes, this method is not suited to study long-lived isomeric states ($\tau > 10^2\mu$s).

A recent new application of this technique has been the study of g factors of isomeric states in neutron-rich nuclei produced by intermediate-energy projectile fragmentation [195]. A cocktail of isomeric projectile fragments can be recoil-separated from most of the other reaction products via an achromatic high-resolution fragment separator. Because the rate of exotic isomers arriving at the focal plane is low, it is not necessary to use a pulsed beam. Instead the isomeric decay is measured by making a correlation between the arrival time of the isomer of interest and the γ decay time. This technique could also be applied to recoil-separated isomers produced by a fusion–evaporation reaction, except that in this case care needs to be taken that noble-gas-like charge states are selected (see section 3.3.1 and later). By using an energy-loss detector with a good energy and time resolution, it is possible to perform an event-by-event ion identification using the energy-loss versus TOF method [196]. With this ion–γ correlation method it is possible to detect every isomeric decay event-by-event and for each isomer individually.

There are several major differences between a TDPAD measurement in an 'in-beam' experiment (after a fusion–evaporation reaction) and in an 'IF' experiment (after a projectile-fragmentation or fusion–evaporation reaction). In 'IF' experiments the isomers are selected through a recoil or fragment separator and transported from the target position to the implantation host. This distance is of the order of several metres and, during their flight, the nuclei are subject to interactions with their surroundings (e.g. external fields, interaction between the electron shell and the nucleus, etc). This gives rise to the following requirements, which are important for the successful application of an 'IF' TDPAD measurement:

1. Only fully stripped ions should be selected by the projectile-fragment separator, or noble gas charge states in case a fusion–evaporation recoil separator is used. If the ions are not fully stripped, the interaction between the electron and the nuclear spins in the atom will induce a considerable decrease up to a complete loss of the nuclear spin-orientation, depending on the charge state of the ions [197, 198]. If a noble gas-like charge state is selected, it is possible to preserve some of the initial orientation [105], sometimes enough to allow a nuclear moment measurement. This is an important option, which needs to be considered for medium and heavy-mass nuclei, where electron pick up processes cannot be neglected in all cases.
2. During the transport of the ions from the production target to the implantation station, the excited nuclear states are decaying. Therefore, the investigated isomeric state cannot have half-lives much shorter than the TOF, which is usually of the order of a few hundred nanoseconds for projectile fragments.
3. Due to rotation of the spin-orientation axis in the dipoles of the mass spectrometer, the alignment axis is not collinear with the beam direction at the implantation point (section 5.2.1). Therefore, the $R(t)$ function needs to be slightly modified to take into

account this effect:

$$R(t,\theta,B) = \frac{I(t,\theta,B) - I(t,\theta+90,B)}{I(t,\theta,B) + I(t,\theta+90,B)} = \frac{3A_2B_2}{4+A_2B_2}\cos\{2(\theta-\gamma_A-\omega_L t)\} \qquad (5.29)$$

Notice that in such an experiment on recoil-separated isomers, not only the frequency of the oscillation depends on the nuclear g factor, but also the phase depends on it through γ_A. In fitting the data this gives an additional restriction, which is important in particular for the study of exotic nuclei where measurements at the limit of statistics are being performed. More details on this type of measurement, including results on g factors in the neutron-rich Ni region can be found in [195, 199].

5.4.2. The LEMS method. The LEMS method was developed about a decade ago [58]. It is a time-integrated combined interaction method, based on the same basic principles as the LMR method. The difference between both methods is that the breaking of the axial symmetry by the combined interaction is on purpose made very strong in a LEMS experiment (by placing a large misalignment angle between the magnetic field and EFG directions or by using a poly-crystalline host). Due to this, it is no longer possible to detect a resonant change in the angular distribution, but rather a 'decoupling' curve is measured. The reason for enhancing the perturbation is to induce a maximum breakdown of the spin-orientation by the quadrupole interaction. By increasing the applied magnetic field strength gradually, a decoupling of both interactions occurs and, at high enough magnetic fields, the initial orientation is restored. The restoration of the initial orientation happens when the ratio of the magnetic to quadrupole interaction frequency fulfills the condition:

$$B(\text{Tesla}) \approx \frac{\nu_Q(\text{MHz})}{3\mu(\mu_N)}$$

For typical quadrupole frequencies of the order of 0.1–10 MHz, and a magnetic moment of the order of 1–10 μ_N, a magnetic field of the order of 0.1–5 T is needed. By measuring a full decoupling curve (called a LEMS-curve), one can fit the ratio of the magnetic moment to the quadrupole moment. If the magnetic moment is known, e.g. from a TDPAD measurement, the quadrupole moment can be deduced. The method is ideally suited to measure the quadrupole moment of long-lived (up to milliseconds) high-spin isomeric states [44], which is not possible with the TDPAD method. A TDPAD quadrupole moment measurement is limited to short-lived isomers ($\tau \sim$ 10–10^3 ns) with low spins. The non-resonant LEMS method is used instead of the resonant γ-LMR method [172], because the latter is not applicable to high-spin states.

The LEMS technique has been applied until now for the in-beam study of fusion–evaporation isomers. Isomeric states in the neutron-deficient Pb region [42–45, 34] as well as K isomers [200] have been investigated successfully.

5.4.3. TF method. The TF method has been developed for the study of g factors of very short-lived isomeric states (10 ps to 1 ns), produced either via fusion–evaporation reactions or via coulomb excitation reactions [190]. The experimental technique, as well as new developments related to the study of short-lived states in exotic radioactive nuclei, have been reviewed by Speidel *et al* [192]. Whereas the first measurements have been performed obviously using stable beams, an enormous boost in the field was initiated during the past few years since rather pure beams of radioactive nuclei have become available and because of the use of advanced high-efficiency γ ray detection systems [201]. The study of ps isomers requires an in-beam measurement of the radioactive γ decay and consequently the study of more exotic isomers

Table 4. Comparison of some properties of techniques for measuring nuclear moments.

Method	Lifetime range	Spin range	Spin-orientation	Radiation	Observable
NMR-ON	>1 s	0.5–...	Alignment/polarization	γ, β	g, Q
β-NMR	1 ms–1 s	0.5–...	Polarization	β	g
β-NQR	1 ms–1 s	1–4	Polarization	β	Q
β-LMR	10 μs–1 s	1–5	Alignment/polarization	β	$Q/\mu, I$
γ-LMR	10 μs–1 s	1–5	Alignment	γ	$Q/\mu, I$
LEMS	100 ns–1 ms	1–...	Alignment	γ	Q/μ
g-TDPAD	10 ns–100 μs	0.5–...	Alignment	γ	g
Q-TDPAD	50 ns–10 μs	1–20	Alignment	γ	Q, I
TF	1 ps–10 ns	0.5–...	Alignment	γ	g

Abbreviations: β-NMR (β-nuclear magnetic resonance), β-NQR (β-nuclear quadrupole resonance), β-LMR (β-level mixing resonance), γ-LMR (γ-level mixing resonance), NMR-ON (nuclear magnetic resonance-on low-temperature oriented nuclei), TDPAD (time differential perturbed angular distribution method), LEMS (level mixing spectroscopy method), TF (transient fields method).

requires the use of techniques to reduce the background, such as the recoil-distance method [202] or the use of perturbed γ coincidence techniques [203, 204] or by selecting a radioactive beam out of the cocktail of reaction products before coulomb-exciting the radioactive beam [205]. Recent g factor measurements on the first excited 2^+ states of radioactive nuclei have been performed, e.g. on the isotopic chains in the Ni-region [206] and in the Kr region [205].

5.5. Regions of applicability and comparison of the methods

In table 4, we give an overview on the regions of applicability for the different methods. We restrict the comparison to methods based on the detection of a perturbation in the angular distribution of the radioactive decay (so excluding the methods based on laser hyperfine structure scans). The applicability of the laser methods is very specific and a variety of such methods has been developed as discussed in section 5.3.1. In comparing the different methods, we will mention the restrictions related to the lifetime of the investigated radioactive species, to their type of radioactive decay, to the type of spin-orientation that is required to apply the method, to the range of nuclear spins that can be investigated and the observable which can be measured. Of course, the regions need to be considered as an approximate order of magnitude, not as exact numbers. The methods that are being compared have been described in the previous sections, or at least references to papers in which more details can be found on these techniques have been given.

6. Conclusions

In this report, we have given an overview on a specific topic which attracts much attention in contemporary nuclear structure research, namely the study of the structure of 'exotic nuclei'. In particular the paper deals with how one can investigate these exotic structures by measuring the static magnetic dipole and electric quadrupole moments of their ground states and excited isomeric states (with lifetimes down to a few picoseconds). The report aims at giving some insight into the nuclear structure properties to which nuclear moments can be sensitive (or not) and to give an overview of the wide variety of experimental techniques that is needed in order to investigate the wide variety of radioactive species, which are now available at several stable and radioactive beam facilities all over the world. An overview on most of the recent developments

in the field of moment measurements on exotic radioactive nuclei has been given, with emphasis on how the new methods are related to recent advances in the production and selection of the radioactive species as well as in the detection systems to look at their radioactive decay.

This field of research has become very active during the past few years (as can be noticed in the reference list) and is still in full development. Because moment measurements require a rather high flux of the radioactive species (typically 10^2–10^5 nuclei s^{-1}) as compared to other spectroscopy methods which require only a few nuclei/minute, the improvement of the radioactive beam intensities will allow these detailed nuclear structure studies to be pushed towards the limits of the nuclear chart, for both the neutron and proton-rich side. The upcoming upgrades of existing facilities and plans for new radioactive beam facilities, providing even more intense beams of very exotic radioactive nuclei, are crucial for this development.

Acknowledgments

I would like to thank everybody who has been member of the LMR team for a stimulating and pleasant collaboration during the past years, as well as all my collaborators around the world who have continuously encouraged me to explore the limits of feasibility for nuclear moment measurements. I acknowledge the FWO-Vlaanderen for my post-doctoral fellowship.

References

[1] Raghavan P 1989 *At. Data Nucl. Data Tables* **42** 189
[2] Stone N 2003 Table of nuclear moments *At. Data Nucl. Data Tables* submitted
[3] Myers W D, Nitschke J M and Norman E B 1990 *1st Int. Conf. on Radioactive Nuclear Beams (Berkeley, USA, 1989)* (Singapore: World Scientific)
[4] Delbar Th 1992 *2nd Int. Conf. on Radioactive Nuclear Beams (Louvain-la-Neuve, Belgium, 1991)* (Bristol: IOP)
[5] Decrock P *et al* 1991 *Phys. Rev. Lett.* **67** 808
[6] Ryckewaert G *et al* 2002 *Nucl. Phys.* A **701** 323c
[7] Villari A C C 2001 *Nucl. Phys.* A **693** 465
[8] Habs D *et al* 1998 *Nucl. Instrum. Methods* B **139** 128
[9] Carter H K *et al* 1997 *Nucl. Instrum. Methods* B **126** 166
[10] Dombsky M *et al* 2000 *Rev. Sci. Instrum.* **71** 978
[11] Tanihata I *et al* 1985 *Phys. Rev. Lett.* **55** 2679
[12] Klotz G *et al* 1993 *Phys. Rev.* C **47** 2502
[13] Tarasov O *et al* 1997 *Phys. Lett.* B **409** 64
[14] Otsuka T *et al* 2001 *Phys. Rev. Lett.* **87** 082502
Otsuka T *et al* 2002 *Eur. Phys. J.* A **13** 69
[15] Caurier E, Nowacki F and Poves A 2001 *Nucl. Phys.* A **693** 374
[16] Samyn M *et al* 2002 *Nucl. Phys.* A **700** 142
[17] Patyk Z *et al* 1999 *Phys. Rev.* C **59** 704
[18] Sakurai H 2002 *Eur. Phys. J.* A **13** 49
[19] Seweryniak D *et al* 2001 *Nucl. Phys.* A **682** 247c
[20] Thibault C *et al* 1975 *Phys. Rev.* C **12** 644
[21] Sarazin F *et al* 2000 *Phys. Rev. Lett.* **84** 5062
[22] Castel B and Towner I S 1990 *Modern Theories of Nuclear Moments (Oxford Studies in Nuclear Physics)* vol 12, ed P E Hodgson (Oxford: Claredon)
[23] Myers W D and Swiatecki W J 1966 *Nucl. Phys.* **81** 1
[24] Heyde K L G 1990 *The Nuclear Shell Model* 2nd edn (Berlin: Springer)
[25] Poppelier N A F M and Glaudemans P W M 1988 *Z. Phys.* A **329** 275
[26] Arima A and Hyuga H 1979 *Mesons in Nuclei* vol 2, ed M Rho and D H Wilkinson (Amsterdam: North-Holland) p 684
[27] Brink D M and Satchler G R 1968 *Angular Momentum* (Oxford: Clarendon)
[28] de-Shalit A and Talmi I 1963 *Nuclear Shell Theory* ed H S W Massey (New York: Academic)
[29] Wouters J, Severijns N, Vanhaverbeke J and Vanneste L 1991 *J. Phys.* G **17** 1673

[30] Bounds J A *et al* 1985 *Phys. Rev. Lett.* **55** 2269
[31] Ekstrom C *et al* 1980 *Nucl. Phys.* A **348** 25
[32] Wallmeroth K *et al* 1987 *Phys. Rev. Lett.* **58** 1516
[33] Pearson M R *et al* 2000 *J. Phys.* G **26** 1829
[34] Vyvey K *et al* 2002 *Phys. Rev. Lett.* **88** 102502
[35] Towner I S, Khanna F C and Hausser O 1977 *Nucl. Phys.* A **277** 285
[36] Stuchbery A E, Byrne A P and Dracoulis G D 1993 *Nucl. Phys.* A **555** 355
[37] Sagawa H and Arima A 1988 *Phys. Lett.* B **202** 15
[38] Becker J A *et al* 1991 *Nucl. Phys.* A **522** 483
[39] Decmann D J *et al Phys. Rev.* C **28** 1060
[40] Ring P and Schuck P 1980 *The Nuclear Many Body Problem* (New York: Springer)
[41] Mahnke H E *et al* 1983 *Phys. Lett.* B **122** 27
[42] Scheveneels G, Hardeman F, Neyens G and Coussement R 1991 *Phys. Rev.* C **43** 2560
[43] Scheveneels G, Hardeman F, Neyens G and Coussement R 1991 *Phys. Rev.* C **43** 2566
[44] Hardeman F *et al* 1991 *Phys. Rev.* C **43** 514
[45] Neyens G *et al* 1993 *Hyperfine Interact.* **78** 195
[46] Kilgallon J *et al* 1997 *Phys. Lett.* B **405** 31
[47] Neyens G *et al* 1997 *Nucl. Phys.* A **625** 668
[48] May A *et al* 1986 *Z. Phys.* A **324** 123
[49] Dracoulis G D *et al* 2001 *Phys. Rev.* C **63** 061302
[50] Vyvey K *et al* 2002 *Phys. Lett.* B **538** 33
[51] Van Duppen P, Coenen E, Deneffe K and Huyse M 1984 *Phys. Rev. Lett.* **52** 1974
[52] Andreyev A N *et al* 2000 *Nature* **405** 430–3
[53] Bengtsson R and Nazarewicz W 1989 *Z. Phys.* **334** 269
[54] Heyde K, Decoster C, Ryckebusch J and Waroquier M 1989 *Phys. Lett.* B **218** 287
[55] Vyvey K *et al* 2002 *Phys. Rev.* C **65** 024320
[56] Eberz J *et al* 1987 *Nucl. Phys.* A **464** 9
[57] Byrne A P *et al* 1990 *Nucl. Phys.* A **516** 145
[58] Hardeman F *et al* 1991 *Phys. Rev.* C **43** 130
[59] Dafni E *et al* 1985 *Phys. Rev. Lett.* **55** 1269
[60] Heyde K 1989 *Mod. Phys.* A **9** 2063
[61] Hübel H 1997 *Prog. Part. Nucl. Phys.* **38** 89
[62] Frauendorf S 2001 *Rev. Mod. Phys.* **73** 463
[63] Clark R M *et al* 1993 *Nucl. Phys.* A **562** 121
[64] Chmel S *et al* 1997 *Phys. Rev. Lett.* **79** 2002
[65] Casten R F and Sherill B M 2000 *Prog. Part. Nucl. Phys.* **45** S171–233
[66] The European isotope separator on-line, http://www.ganil.fr/eurisol/
[67] The rare isotope accelerator, http://www.phy.anl.gov/ria/index.html
[68] Tanihata I 1995 RI beam factory project *Nucl. Phys.* A **588** 253c
[69] Geissel H, Munzenberg G and Riisager K 1995 *Ann. Rev. Nucl. Part. Sci.* **45** 163–203
[70] Simpson J 1997 *Z. Phys.* A **358** 139–43
[71] Lee I 1992 *Prog. Part. Nucl. Phys.* **28** 473
Lee I 1997 *Prog. Part. Nucl. Phys.* **38** 65
[72] Vetter K *et al* 2000 *Nucl. Instrum. Methods* A **452** 105
[73] Lieder R M *et al* 2001 *Prog. Part. Nucl. Phys.* **46** 399
[74] Morinaga H and Yamazaki T 1976 *In-beam Gamma-ray Spectroscopy* (Amsterdam: North-Holland)
[75] Steffen R M and Alder K 1975 *The Electromagnetic Interaction in Nuclear Spectroscopy* (Amsterdam: North-Holland)
[76] Alder K *et al* 1956 *Rev. Mod. Phys.* **28** 432
[77] Lecomte R *et al* 1980 *Phys. Rev.* C **22** 2420
[78] Huyse M 2002 *Nucl. Phys.* A **701** 265C
[79] Ravn H L 1979 *Phys. Rep.* **54** 201
[80] Ravn H, Sundell S and Westgaard L 1975 *Nucl. Instrum. Methods* **123** 131
[81] Arje J *et al* 1986 *Nucl. Instrum. Methods* A **247** 431
[82] Deneffe K *et al* 1987 *Nucl. Instrum. Methods* B **26** 399
[83] Xu H J *et al* 1993 *Nucl. Instrum. Methods* A **333** 274
[84] VandenBergh P *et al* 1997 *Nucl. Instrum. Methods* B **126** 194
[85] Dendooven P *et al* 1998 *Nucl. Instrum. Methods* A **408** 530

[86] Cooke J L *et al* 1997 *J. Phys.* G **23** L97
[87] Alkhzov G D, Berlovich E Y and Panteleyev V N 1989 *Nucl. Instrum. Methods* A **280** 141
[88] Michin V I *et al* 1993 *Nucl. Instrum. Methods* B **73** 550
[89] Vermeeren L *et al* 1994 *Phys. Rev. Lett.* **73** 1935
[90] Huyse M, Facina M, Kudryavtsev Y and Van Duppen P 2002 *Nucl. Instrum. Methods* B **187** 535
[91] Savard G *et al* 2002 *Contribution to EMIS (Victoria, BC, Canada, 5—11 May 2002)* vol XIV
[92] Spolaore P *et al* 1985 *Nucl. Instrum. Methods* A **238** 381
[93] Davids C N *et al* 1992 *Nucl. Instrum. Methods* B **70** 358
[94] Leino M *et al* 1995 *Acta Phys. Pol.* B **26** 309
[95] Nisius D *et al* 1993 *Phys. Rev.* C **47** 1929
[96] Spolaore P *et al* 1995 *Nucl. Instrum. Methods* A **395** 500
[97] Paul E S *et al* 1995 *Phys. Rev.* C **51** 78
[98] de France G 1999 *Acta Phys. Pol.* B **30** 1661
[99] Simpson J *et al* 2000 *Acta Phys. Hungaria, Heavy Ion Phys.* **11** 159
[100] Mittig W 1998 *J. Phys.* G **24** 1331
[101] Datz S 1975 *Phys. Scr.* **11** 149
[102] Broude C *et al* 1973 *Nucl. Phys.* A **215** 617
[103] Brenn R *et al* 1977 *Z. Phys.* A **281** 219
[104] Neyens G, Nouwen R and Coussement R 1994 *Nucl. Instrum. Methods* A **340** 555
[105] Dafni E and Satteson M 1988 *Phys. Rev.* C **38** 2949
[106] Leino M 1997 *Nucl. Instrum. Methods* B **126** 320
[107] Brenn R, Hopkins F and Sprouse G D 1978 *Phys. Rev.* A **17** 1837
[108] Levy R, Benczer Koller N, Broude C and Hagemeyer K 1981 *Z. Phys.* A **301** 243
[109] Summerer K and Blank B 2000 *Phys. Rev.* C **61** 034607
[110] Bernas M *et al* 1997 *Nucl. Phys.* A **616** 352c
[111] Bazin D, Tarazon O, Lewitowicz M and Sorlin O 2002 *Nucl. Instrum. Methods* A **482** 307
[112] Anne R *et al* 1987 *Nucl. Instrum. Methods* A **257** 215
[113] Sherrill B M, Morrissey D J and Nolan J A *et al* 1991 *Nucl. Instrum. Methods* B **56** 1106
[114] Geissel H *et al* 1992 *Nucl. Instrum. Methods* B **70** 286
[115] Kubo T *et al* 1992 *Nucl. Instrum. Methods* B **70** 309
[116] Mueller A C and Anne R 1991 *Nucl. Instrum. Methods* B **56** 559
[117] Kopf U *et al* 1969 *Z. Phys.* **226** 297
[118] Happer W 1972 *Rev. Mod. Phys.* **44** 169
[119] Huber G, Bonn J, Kluge H J and Otten E W 1976 *Z. Phys.* A **276** 187
[120] Fisher H *et al* 1978 *Z. Phys.* A **284** 3
[121] Arnold E *et al* 1987 *Phys. Lett.* B **197** 311
Arnold E *et al* 1988 *Z. Phys.* A **331** 295
[122] Geithner W *et al* 1999 *Phys. Rev. Lett.* **83** 3792
[123] Postma H and Stone N J (ed) 1986 *Low Temperature Nuclear Orientation* (Amsterdam: North-Holland)
[124] Wu C *et al* 1957 *Phys. Rev.* C **105** 1413
[125] Neyens G, S'Heeren G and Coussement R 1997 *Nucl. Instrum. Methods* B **122** 121
[126] Goldring G 1992 *Hyperfine Interact.* **75** 355
[127] Hass M *et al* 1991 *Phys. Rev.* C **43** 2140
[128] Nojiri Y and Deutch B I 1983 *Phys. Rev. Lett.* **51** 180
[129] Lu F Q, Tang J Y and Deutch B I 1982 *Phys. Rev.* C **25** 1476
[130] Schroder H and Kupper E 1976 *Z. Phys.* A **279** 13
[131] Davni E *et al* 1993 *Phys. Rev. Lett.* **50** 1652
[132] Lindroos M *et al* 1995 *Nucl. Instrum. Methods Phys. Res.* A **361** 53
[133] Borremans D *et al* 2002 *Phys. Rev.* C 054601
[134] Correll F D *et al* 1983 *Phys. Rev.* C **28** 862
[135] Minamisono T *et al* 1975 *Phys Rev. Lett.* **34** 1465
[136] Minamisono T *et al* 1976 *Phys. Rev.* C **14** 376
[137] Butler P A and Nolan P J 1981 *Nucl. Instrum. Methods* **190** 283
[138] Newton J O *et al* 1967 *Nucl. Phys.* A **95** 357
[139] Williams R L Jr, Pfeiffer L, Wells J C Jr and Madansky L 1970 *Phys. Rev.* C **2** 1219
[140] Asahi K *et al* 1984 *Nucl. Instrum. Methods* **220** 389
[141] Asahi K *et al* 1991 *Phys. Rev.* C **43** 456
[142] Schmidt-Ott W D *et al* 1994 *Z. Phys.* A **350** 215

[143] Neyens G *et al* 1997 *Phys. Lett.* B **393** 36
[144] Asahi K *et al* 1990 *Phys. Lett.* B **251** 488
[145] Mantica P F *et al* 1999 *Nucl. Instrum. Methods* A **422** 498
[146] Schafer M *et al* 1998 *Phys. Rev.* C **57** 2205
[147] Smith A G *et al* 1999 *Phys. Rev.* C **6006** 4611
[148] Smith A G *et al* 1999 *Phys. Lett.* B **453** 206
[149] Anton K R *et al* 1978 *Phys. Rev. Lett.* **40** 642
[150] Neugart R 1981 *Nucl. Instrum. Methods Phys. Res.* **186** 165
[151] Otten E W 1989 *Treatise on Heavy-Ion Science* vol 8, ed D A Bromley (New York: Plenum)
[152] Boos N *et al* 1994 *Phys. Rev. Lett.* **72** 2689
[153] Billowes J and Campbell P 1995 *J. Phys.* G **21** 707
[154] Levins J M G *et al* 1999 *Phys. Rev. Lett.* **82** 2476
[155] Coulier N *et al* 2001 *Phys. Rev.* C **63** 054605 (7 p)
[156] Rossini F A and Knight W D 1969 *Phys. Rev.* **178** 641
[157] Riegel D 1975 *Phys. Scr.* **11** 228
[158] Korringa J 1950 *Physica* **XVI** 601
[159] Hume-Rothery W, Smallman R E and Haworth C W 1969 *Structure of Metals and Alloys* (London: Institute of Metals)
[160] Ternier S *et al* 1998 *Nucl. Instrum. Methods* B **140** 235
[161] Matthias E *et al* 1971 *Phys. Rev.* A **4** 1626
[162] Okuno H *et al* 1995 *Phys. Lett.* B **354** 41
[163] Borremans D *et al* 2002 *Phys. Lett.* B **537** 45
[164] Coulier N *et al* 1999 *Phys. Rev.* C **59** 1935
[165] Neyens G *et al* 1999 *Phys. Rev. Lett.* **82** 497
[166] Kaufmann E N and Vianden R J 1979 *Rev. Mod. Phys.* **51** 161
[167] Arnold E *et al* 1992 *Phys. Lett.* B **281** 16
[168] Minamisono T *et al* 1992 *Phys. Rev. Lett.* **69** 2058
[169] Matthias E *et al* 1962 *Phys. Rev.* **125** 261
[170] Coussement R, Put P, Scheveneels G and Hardeman F 1985 *Hyperfine Interact.* **23** 273
[171] Gaziorowicz S (ed) 1974 *Quantum Physics* (New York: Wiley)
[172] Scheveneels G, Hardeman F, Neyens G and Coussement R 1989 *Hyperfine Interact.* **52** 273
[173] Schweikhard L and Kluge H-J (ed) 2000 *Proc. 1st Euroconf. on Atomic Physics at Accelerators (APAC'99): Laser Spectroscopy and Applications*, *Hyperfine Interact.* vol 127, pp 1–543
[174] Le Blanc F 2000 *Hyperfine Interact.* **127** 71
[175] Leblanc F *et al* 1997 *Phys. Rev. Lett.* **79** 2213
Leblanc F *et al* 1999 *Phys. Rev.* C **6005** 4310
[176] Nieminen A *et al* 2002 *Phys. Rev. Lett.* **88** 094801
[177] Campbell P *et al* 2002 *Phys. Rev. Lett.* **89** 082501
[178] Koster U *et al* 2000 *Hyperfine Interact.* **127** 417
[179] Weissman L *et al* 2002 *Phys. Rev.* C **65** 024315
[180] Andreyev A N *et al* 2002 *Eur. Phys. J.* A **14** 63
[181] Keim M *et al* 2000 *Eur. Phys. J.* A **8** 31
[182] Nojiri Y, Takeyama K, Matsuta K and Minamisono T 1987 *Hyperfine Interact.* **35** 1015
[183] Stone N J 1985 *Hyperfine Interact.* **22** 3
[184] Wouters J *et al* 1986 *Phys. Rev. Lett.* **56** 1901
[185] Schuurmans P *et al* 1996 *Phys. Rev. Lett.* **77** 4720
[186] Kraus J *et al* 1998 *Phys. Rev.* C **58** 3181
[187] Stone N J *et al* 1999 *Hyperfine Interact.* **121** 645
[188] White G N *et al* 1999 *Hyperfine Interact.* **121** 651
[189] Rikovska J 2000 *Phys. Rev. Lett.* **85** 1392
[190] Benczer-Koller N *et al* 1980 *Ann. Rev. Nucl. Part. Sci.* **30** 53–84
[191] Hausser O *et al* 1980 *Nucl. Instrum. Methods* **169** 539
[192] Speidel K-H, Kenn O and Nowacki F 2002 *Prog. Part. Nucl. Phys.* **49** 91–154
[193] Goldring G and Hass M 1985 *Treaties on Heavy Ion Science* vol 3, ed D Allan Bromley (New York: Plenum) p 539
[194] Christiansen J *et al* 1970 *Phys. Rev.* C **1** 613
[195] Georgiev G *et al* 2002 *J. Phys.* G **28** 2993–3006
Georgiev G *et al* 2001 *Phys. At. Nuclei* **64** 1181–5

[196] Bazin D *et al* 1990 *Nucl. Phys.* A **515** 349
[197] Goldring G 1982 *Heavy Ion Collisions* ed R Bock (Amsterdam: North-Holland) p 483
[198] Vyvey K *et al* 2000 *Phys. Rev.* C **62** 034317
[199] Neyens G *et al* 2002 *Nucl. Phys.* A **701** 403
[200] Balabanski D L *et al* 2001 *Phys. Rev. Lett.* **86** 604
[201] Jungclaus A *et al* 1997 *Prog. Part. Nucl. Phys.* **38** 87
[202] Jungclaus A *et al* 1998 *Phys. Rev. Lett.* **80** 2793
[203] Stuchbery A E 2002 *Nucl. Instrum. Methods* A **485** 753
[204] Patel D *et al* 2002 *J. Phys.* G **28** 649
[205] Mertzimekis T J *et al* 2001 *Phys. Rev.* C **64** 024314
[206] Kenn O *et al* 2001 *Phys. Rev.* C **63** 064306
Kenn O *et al* 2002 *Phys. Rev.* C **65** 034308